SKELETAL MUSCLE HOMEOSTASIS IN

GOLDEN RETRIEVER MUSCULAR DYSTROPHY:

THE ROLE OF APOPTOSIS & AUTOPHAGY IN GRMD PATHOGENESIS

A Dissertation

by

WILLIAM BENJAMIN STOUGHTON

Submitted to the Office of Graduate and Professional Studies of
Texas A&M University
in partial fulfillment of the requirements for the degree of

DOCTOR OF PHILOSOPHY

Chair of Committee,	Joe N. Kornegay
Committee Members,	Jianrong Li
	Noah D. Cohen
	Scott Dindot
	Candice Brinkmeyer-Langford
Head of Department,	Evelyn Castiglioni

December 2016

Major Subject: Biomedical Sciences

ABSTRACT

Duchenne muscular dystrophy (DMD) is an X-linked recessive genetic disorder caused by mutations in the *DMD* gene, which results in loss of the dystrophin protein and cyclic muscle degeneration and regeneration. The main animal models include the mdx mouse and golden retriever muscular dystrophy (GRMD) dog. Dogs with GRMD have more severe disease than mice, in keeping with DMD. Variable disease expression in GRMD at the individual and muscle level provides an excellent platform to study the pathophysiology of muscular dystrophy beyond the primary effects of dystrophin loss. Autophagy and apoptosis have recently been identified as suitable secondary therapeutic targets. We sought to explore their role in GRMD pathogenesis through gene and protein expression assays and light and transmission electron microscopy.

Our initial studies focused on expression of an anti-apoptotic protein, APIP, in the differentially affected cranial sartorius (CS) and vastus lateralis (VL) muscles. We hypothesized that inhibition of apoptosis by APIP would be beneficial but, instead, found that VL protein levels tracked with a more severe phenotype. APIP was primarily expressed in regenerating fibers and inflammatory cells, perhaps providing an additional clue to its role in dystrophic muscle. Expression in regenerating fibers could be tied to anti-apoptotic activity or methionine metabolism.

Next, we investigated the role of autophagy, again focusing on the CS and VL. We hypothesized that autophagy would be reduced in GRMD muscle and be characterized by lower autophagy gene and protein (i.e., LC3B-II) expression and higher p62 levels. FOXO3 regulated genes were lower than normal in the GRMD CS, however

contrary to our hypothesis, LC3B-II and p62 levels were higher in the dystrophic muscle, indicating impaired autophagy which correlated with a more severe phenotype. Autophagic structures were found in necrotic myofibers and inflammatory cells, suggesting dual roles. Treatment with an NF-κB inhibitor activated autophagy gene expression in a muscle-dependent way in treated GRMD dogs, generally in line with an improved phenotype.

In summary, apoptosis and autophagy are important in maintaining muscle homeostasis in the GRMD dog. Future studies are required to determine how APIP influences muscle regeneration and how autophagy activation can modulate GRMD pathogenesis.

DEDICATION

This work is dedicated to the many children and families afflicted with Duchenne muscular dystrophy. My hope and prayer is that this work may aid the discovery of new treatments and someday, even a cure for this debilitating disease.

ACKNOWLEDGEMENTS

I would like to thank my committee chair, Dr. Joe Kornegay, and my committee members, Dr. Cohen, Dr. Li, Dr. Brinkmeyer-Langford, and Dr. Dindot, for their friendship, guidance and support throughout the course of this research. I have learned so much over the past 4 ½ years and am indebted to you all. I sincerely hope and pray that I can serve the students I mentor in the future as well as you have served me.

Special thanks is needed for Dr. Joe Kornegay, who spent countless hours reading my scientific 'novels'. Without his knowledge, support, persistence, motivation, patience, and honest critique of my work, this dissertation would never have been completed.

Thanks also go to my friends and colleagues and the VIBS department faculty and staff for making my time at Texas A&M University a great experience. I will wear my Aggie Ring with pride and strive to represent the core values of Texas A&M in all that I do.

Thanks to my mother and father for their prayers and frequent words of encouragement and to my wonderful, thoughtful wife Aubrey and our children for their patience and love. Finally, I thank my Lord and Savior Jesus Christ for His love, grace and mercy, who without His special care I would not have been able to complete the 31st grade.

CONTRIBUTORS AND FUNDING SOURCES

Contributors

This work was supervised and supported by a dissertation committee consisting of Professor Joe Kornegay, Dr. Jianrong Li and Dr. Candice Brinkmeyer-Langford of the Department of Veterinary Integrative Sciences (VIBS), and Dr. Scott Dindot of the Department of Veterinary Pathobiology, and Dr. Noah Cohen of the Department of Large Animal Clinical Sciences.

Transmission electron microscopy work for Section 3 was provided with the assistance of Dr. Ross Payne at Texas A&M University College of Veterinary Medicine Image Analysis Laboratory-Electron Microscopy Division. Gene expression and western blotting for sections 2, 3, and 4 were completed with the assistance of Cindy Balog-Alvarez in the VIBS Department. Identification of APIP as a candidate modifier gene in GRMD was directed by Dr. Candice Brinkmeyer-Langford in the VIBS Department. All other work conducted for the dissertation was completed by the student independently.

Funding Sources

My graduate study was funded through a start-up package to Dr. Joe Kornegay and by the College of Veterinary Medicine & Biomedical Sciences (CVM) at Texas A&M University Graduate Merit Scholar Fellowship.

NOMENCLATURE

DMD	Duchenne muscular dystrophy
GRMD	Golden retriever muscular dystrophy
CS	Cranial sartorius
VL	Vastus lateralis
CT	Cranial tibialis
MHG	Medial head of gastrocnemius
NBD	Nemo binding domain peptide
APIP	APAF-1 interacting protein
UPS	Ubiquitin-proteasome system
LC3B	Microtubule-associated proteins 1A/1B light chain 3B
p62	Sequestosome-1
MHC	Myosin heavy chain
DGC	Dystrophin glycoprotein complex
APAF1	Apoptotic peptidase activating factor 1 protein
BCL2	B-cell lymphoma 2 protein
BAX	BCL2 associated X protein
TTJ	Tibiotarsal joint
TJA	Tibiotarsal joint angle
NF-κB	Nuclear factor-κB
IKK	Inhibitor of kappa B kinase complex

TABLE OF CONTENTS

Page

LIST OF FIGURES

Page

LIST OF TABLES

Page

1. INTRODUCTION

1.1 Background of Duchenne Muscular Dystrophy

Duchenne muscular dystrophy (DMD) is an X-linked neuromuscular disorder that occurs due to mutations in the *DMD* gene in approximately 1:4000 to 1:5000 male births [1]. The mutation typically results in the absence of a functional dystrophin protein. Dystrophin is a key component of the dystrophin-glycoprotein complex (DGC), which is critical for linking the muscle cytoskeleton to the extracellular matrix [2]. When dysfunctional, a complex cycle of progressive muscle degeneration leads to eventual muscle fibrosis, wheelchair confinement, recumbency, and terminal respiratory and/or cardiovascular failure. Currently, therapies are primarily palliative in nature and often include anti-inflammatory medications (e.g., corticosteroids) and physical therapy. Corticosteroids, which are now essentially the standard of care for DMD, can only slow the destructive cyclical muscle pathology [3]. While gene and cell-based therapies that offer a potential cure are being pursued in animal models (e.g., mouse and canine) and DMD clinical trials, there is also considerable interest in reducing the so-called secondary effects of dystrophin loss. Identification of therapeutics that could lessen fibrosis, inflammation, and accumulation of damaged proteins and organelles (e.g., autophagy), without the side effects of corticosteroids, remains an important objective in DMD research.

1.2 Background of Golden Retriever Muscular Dystrophy

The 2 primary animal models used to perform preclinical trials and investigate the pathophysiology of dystrophinopathies are the mouse (mdx) and dog. Our laboratory focuses primarily on identifying early clinical biomarkers and performing preclinical trials in the canine model of DMD, specifically known as golden retriever muscular dystrophy (GRMD) [4]. The genetic defect in the GRMD dog, which leads to the absence of dystrophin, is caused by a single nucleotide transition mutation at the 3' consensus splice site of intron 6 [5]. This results in exon 7 being skipped and a reading frame shift, which leads to a premature stop codon in exon 8. Advantages to utilizing the GRMD model include its similar phenotype to DMD and patterns of pathology that parallel those in DMD.

Despite the fact that all DMD patients and animal models have mutations in the *DMD* gene, tremendous phenotypic variation exists at 4 levels: species, individual, muscle, and fiber type. The cause for this variation can be attributed to several factors including the type and location of the mutation within the *DMD* gene and the potential for modifier genes to either improve or worsen the phenotype. The type and location of the mutation (most commonly a variably-sized deletion) has classically been associated with 2 general forms of dystrophin deficient muscular dystrophy, namely the more severe DMD and the milder Becker Muscular Dystrophy (BMD)[6]. In DMD, the mutation in the *DMD* gene results in premature termination of transcription due to a shift in the reading frame. Little or no stable, functional protein is produced and the classically more severe DMD phenotype occurs. In BMD, the *DMD* gene mutation

maintains the reading frame, allowing production of a truncated, yet functional dystrophin protein that effectively joins the DGC to stabilize the muscle cell membrane. Anti-sense oligonucleotides are currently being investigated as a mechanism by which exon skipping and restoration of the reading frame can be achieved, thereby allowing a DMD patient to produce a truncated dystrophin, with associated clinical improvement to a BMD-like phenotype.

Genetic modifiers are important contributors to the phenotypic variation identified in DMD. The investigation for these modifiers historically has included expression assays (e.g., microarray) and quantitative PCR in both DMD and animal dystrophinopathies. As would be expected, genes related to muscle regeneration and inflammation have often been upregulated in these studies. Correlating gene expression with 1 or more phenotypic features, suggesting a cause-and-effect relationship, strengthens such studies. Another method of identifying genetic modifiers entails a genome wide association study (GWAS) that uses single nucleotide polymorphisms (SNPs) and linkage disequilibrium to identify blocks of the genome that may be associated with phenotype. Recently, latent transforming growth factor beta binding protein 4 (*LTBP4*) and secreted phosphoprotein 1 (*SPP1*) have been defined as potential genetic modifiers in DMD patients with variable disease severity [7-9].

The phenotypic variation in the GRMD dog provides a unique opportunity to investigate the pathophysiology of muscular dystrophy and the role of genetic modifiers. Within a litter of GRMD dogs, there can be both mildly and severely affected dogs that all have the same *DMD* gene mutation. Furthermore, GRMD dogs display remarkable

phenotypic variation at the muscle level, for example the cranial sartorius (CS) undergoes early necrosis and hypertrophy, whereas the vastus lateralis (VL) undergoes delayed necrosis and atrophy [10, 11]. Recently, the *Jagged1* gene was identified as a candidate genetic modifier of GRMD, with overexpression improving the dystrophic dog phenotype [12]. The identification and characterization of genetic modifiers will continue to provide further insight into DMD pathogenesis, potentially identifying therapeutic targets and allowing for better clinical trial stratification.

1.3 The Role of Apoptosis in Skeletal Muscle Homeostasis

Duchenne muscular dystrophy is a debilitating condition without sufficient therapeutic options and an ultimately fatal disease course. The pathophysiology associated with DMD, although still debated, can be attributed to myofiber membrane instability, accumulation of reactive oxygen species and damaged organelles, intracellular Ca^{+} mishandling, and, finally, muscle cell death with secondary inflammation and fibrosis [13, 14]. Potential cures, such as *DMD* gene therapy, are not currently available. Therefore, it is important to continue the pursuit of novel adjunctive therapies that can modulate the phenotype without replacing dystrophin. Given that anti-inflammatory medications (e.g., corticosteroids) can slow the disease progression, it appears the secondary tissue response is of great importance in determining the severity of the disease [3]. Investigating the complex role of cell death and survival mechanisms is crucial for elucidating the progressive muscle degeneration that occurs beyond the primary disease response to the loss of dystrophin.

Briefly, apoptosis (i.e., programmed cell death) is an essential physiological process required for normal tissue development and cellular homeostasis. There are 2 classical ways by which programmed cell death occurs, the extrinsic and intrinsic apoptotic pathways. The extrinsic pathway involves plasma membrane signaling through the tumor necrosis factor-receptor family and activation of caspase-8 [15]. The intrinsic pathway is triggered to initiate cell death by an imbalance in anti-apoptotic (e.g., B-cell lymphoma 2 [BCL2]) and pro-apoptotic (e.g., BCL2-associated X protein [BAX]) signals. Once initiated, mitochondrial membrane pore permeability increases and the caspase-activating factor cytochrome C is released into the cytoplasm [16]. The ensuing cascade of caspases, starting with caspase-9, results in formation of the apoptosome through interaction with apoptotic peptidase activating factor 1 (APAF-1) [15]. The apoptosome then orchestrates cellular breakdown without the release of noxious cellular constituents [16]. Although apoptosis is known to occur in dystrophinopathies, the triggering events that lead to muscle-fiber apoptosis are ill-defined [17].

Any individual cell is constantly balancing pro-apoptotic (e.g., BAX) and anti-apoptotic (e.g., BCL2) signals during growth, maintenance, and disease. Inhibition of cell death mechanisms at various stages continues to be investigated in dystrophic animal models. Studies in the mdx mouse have produced conflicting results. One concluded that increased expression of BCL2 did not improve the phenotype significantly [18]. However, 2 recent studies showed that inhibition of the intrinsic apoptotic pathway at the mitochondrial pore level did improve the mdx phenotype [19,

20]. Therefore, it appears that modulation of the apoptotic pathway could play an important role in DMD pathophysiology and further investigation could reveal novel therapeutic targets.

1.4 The Role of Autophagy in Skeletal Muscle Homeostasis

Macroautophagy (hereafter known as autophagy) is a conserved biological mechanism found in all eukaryotic cells that involves “self-eating”. Autophagy is an essential survival mechanism, which allows for the recycling of cellular building blocks by organized degradation of selected proteins and organelles into macromolecules [21]. Autophagy is also critical for the quality control of mitochondria, which helps ensure that damaged mitochondria do not persist in the cell and contribute to excessive oxidative stress [22]. Autophagy is now associated with numerous pathophysiological processes, including cancer, neurodegenerative disorders, cardiovascular disease, and even normal physiological processes like aging and exercise [23]. This multi-step cellular process requires a functional lysosomal system and coordination of over 30 different proteins [24]. Briefly, the tagged cytoplasmic contents (e.g., damaged proteins and organelles) are captured and carefully enclosed into the autophagosome. The autophagosome, which contains the cargo collected for recycling, then binds to the lysosome forming the autolysosome. The autolysosome degrades the cargo utilizing lysosomal hydrolases and subsequently releases the resulting macromolecules for re-use by the cell.

Dysregulation at any of these steps can affect tissue homeostasis and contribute to disease. Post-mitotic cells (e.g., myofibers and neurons) are more susceptible to disruptions in autophagy, which can ultimately lead to the accumulation of excessive cellular ‘garbage’ (i.e., damaged/toxic proteins and organelles) and cellular senescence [25]. Skeletal muscle is a post-mitotic tissue that depends primarily on satellite cells for regeneration and tissue repair [26]. Autophagy can be a double-edged sword in skeletal muscle, with either too much or too little resulting in muscle atrophy and cell death [27, 28]. Therefore, the tight regulation of autophagy is critical for maintaining muscle homeostasis.

The variable phenotype found between individual GRMD dogs and muscle types (e.g., flexors and extensors) provides a unique opportunity to investigate the role of these homeostatic mechanisms in dystrophinopathies. In general, the mdx literature suggests that inhibition of apoptosis and activation of autophagy would be beneficial. However, prior to therapeutic modulation of apoptosis and autophagy in DMD boys, these assumptions should be validated in the GRMD dog. Therefore, we elected to investigate the role of these homeostatic mechanisms in GRMD pathogenesis and focused on the CS and VL, which are differentially affected.

2. APIP EXPRESSION IS ASSOCIATED WITH GRMD PHENOTYPE

2.1 Introduction

Duchenne muscular dystrophy (DMD) is an X-linked genetic disorder, affecting approximately 1:4000 to 1:5000 live male births [1]. DMD is caused by mutations in the *DMD* gene, which results in the absence of the protein dystrophin. Dystrophin is a key component of the dystrophin-glycoprotein complex (DGC) and is critical in cell signaling and linking the muscle cytoskeleton to the extracellular matrix [2]. Without dystrophin, skeletal muscle undergoes progressive cycles of degeneration and regeneration with subsequent fibrosis, weakness, and debilitating contractures. This complex cycle of muscle damage eventually leads to wheelchair confinement, recumbence, and terminal respiratory and/or cardiovascular failure. Despite discovery of the causative genetic mutation in DMD ~ 30 years ago, there is no cure for this fatal disease, and an urgent demand remains for development of novel therapeutics.

The 2 primary animal models used to perform preclinical trials and investigate the pathophysiology of dystrophinopathies are the mouse (mdx) and dog. Our laboratory focuses primarily on identifying early clinical biomarkers and performing preclinical trials in the canine model of DMD, specifically known as Golden retriever muscular dystrophy (GRMD) [4]. The genetic defect in the GRMD dog, which leads to the absence of dystrophin, is caused by a single nucleotide transition mutation at the 3' consensus splice site of intron 6 [5] of the *DMD* gene. This results in exon 7 being skipped and a reading frame shift, with a resulting premature stop codon in exon 8.

Because the GRMD phenotype more closely mirrors that of DMD when compared to the mdx mouse, mechanistic and preclinical treatment studies may be more likely to translate to humans.

Despite the fact that all DMD patients and animal models have mutations in the *DMD* gene, tremendous phenotypic variation exists at 4 levels: species, individual, muscle, and fiber type. The cause for this variation can be attributed to several factors, including the type and location of the mutation within the *DMD* gene and the potential for modifier genes to either improve or worsen the phenotype. The type and location of the mutation (most commonly a variably-sized deletion) has classically been associated with 2 general forms of dystrophin deficient muscular dystrophy, namely the more severe DMD and the milder Becker muscular dystrophy (BMD)[6]. The *DMD* gene mutation causes a shift of the reading frame and premature termination of transcription. Little or no stable, functional protein is produced and the classically more severe DMD phenotype occurs. The BMD mutation maintains the reading frame, allowing production of a truncated, yet functional dystrophin protein that effectively joins the DGC to stabilize the muscle cell membrane. Anti-sense oligonucleotides are currently being investigated as a mechanism by which exon skipping and restoration of the reading frame can be achieved, thereby allowing a DMD patient to produce a truncated dystrophin, with conversion to a milder BMD-like phenotype [29, 30].

Genetic modifiers are important contributors to the phenotypic variation identified in DMD. These modifiers have historically been studied using expression assays (e.g., microarray) and quantitative PCR in both DMD and animal

dystrophinopathies. As would be expected, genes related to muscle regeneration and inflammation have often been up-regulated, while those involved in metabolism have been down-regulated [31-33]. Correlating gene expression with 1 or more phenotypic features, suggesting a cause-and-effect relationship, strengthens such studies. Another method of identifying genetic modifiers entails a genome-wide association study (GWAS) that uses single nucleotide polymorphisms (SNPs) and linkage disequilibrium to identify blocks of the genome that may be associated with phenotype. Recently, latent transforming growth factor beta binding protein 4 (*LTBP4*) and secreted phosphoprotein 1 (*SPP1*) have been defined as potential genetic modifiers in DMD patients with variable disease severity [7-9].

The phenotypic variation in the GRMD dog provides a unique opportunity to investigate the pathophysiology of muscular dystrophy and the role of genetic modifiers. Within a litter of GRMD dogs, there can be both mildly and severely affected dogs that all have the same *DMD* gene mutation. Furthermore, GRMD dogs display remarkable phenotypic variation at the muscle level; for example, the cranial sartorius (CS) undergoes early necrosis and hypertrophy, whereas the vastus lateralis (VL) undergoes delayed necrosis and atrophy [10, 11]. Recently, the *Jagged1* gene was identified as a candidate genetic modifier of GRMD, with expression of a particular allele tracked to an outcross improving the dystrophic dog phenotype [12]. The identification and characterization of genetic modifiers will continue to provide further insight into DMD pathogenesis, potentially identifying therapeutic targets and allowing for better clinical trial stratification. In a recent GRMD genome-wide association study from our

laboratory, several candidate genetic modifiers associated with phenotype were identified [34]. Based on these results, we elected to pursue protein expression studies on 3 candidate genetic modifiers: a) APAF-1 interacting protein (APIP); b) peptidase domain containing associated with muscle regeneration 1 (PAMR1); and, c) peptidylprolyl isomerase A (PPIA). Preliminary protein expression studies narrowed our focus to APIP as a genetic modifier in GRMD.

APIP has at least 2 unique functions relating to its anti-apoptotic and enzymatic activities (e.g., methionine metabolism) that could be relevant to muscle disease. APIP inhibits programmed cell death (i.e., apoptosis) through direct interaction with APAF-1, an activator of caspase-9 essential for apoptosome formation [35, 36]. In contrast to cell necrosis, apoptosis is a tightly regulated process by which cells that threaten or are no longer needed can be destroyed without spilling their contents and inducing inflammation. In one sense, apoptosis is the more 'beneficial' way for cells to die. While necrosis is the terminal mechanism of cell death in DMD [37], the intrinsic apoptotic pathway is also activated in DMD myofibers in advance of necrosis [14]. Indeed, the fact that APAF-1 is decreased in skeletal muscle of DMD and BMD patients [38] could relate to APIP's interaction to inhibit apoptosome formation. APIP's predominant expression in regenerating myofibers suggests a potential alternative role in preventing myoblast death, similar to the anti-apoptotic factor BCL2 [39, 40].

In order to investigate the role of APIP in GRMD pathogenesis and further validate our GWAS findings, protein expression was studied in the phenotypically distinct CS and VL muscles at 6 months of age, when functional studies tend to correlate

[41-43]. Interestingly, APIP protein was differentially expressed in the GRMD versus normal VL but not in the GRMD CS. Levels in the dystrophic VL correlated positively with a more severe phenotype, perhaps pointing to a causal relationship. APIP expression was localized to regenerating myofibers in dystrophic muscle suggesting a role in muscle repair. Further investigation is required to elucidate the impact of APIP on the regenerative response of dystrophic muscle.

2.2 Materials and Methods

2.2.1 Animals

Dogs used in these studies were from a colony at the University of North Carolina at Chapel Hill (UNC-CH) that was subsequently moved to Texas A&M University (TAMU). They were cared for and assessed according to principles outlined in the National Research Council Guide for the Care and Use of Laboratory Animals. Natural history studies performed at UNC-CH were approved by the UNC-CH Institutional Animal Care and Use Committee (IACUC) through protocol, Natural History and Immunological Parameters in the German Shorthaired Pointer Muscular Dystrophy (GSHPMD) Dog (09-011). Animal care and biomarkers used to characterize phenotype were covered by the IACUC protocol, Standard Operating Procedures—Canine X-Linked Muscular Dystrophy (09-351). Persistence of the *DMD* splice site mutation in all GRMD dogs and carriers of our colony was confirmed by performing a restriction fragment length polymorphism (RFLP) analysis (Sau96) and sequencing the isolated PCR product region of the intron 6-exon 7 splice site as previously described

(data not shown) [5, 44].

Phenotypic data were collected through a natural history study that included 10 untreated GRMD dogs and 8 age-matched wild type littermates. Samples of the CS and VL were collected at 6 months of age by either biopsy or necropsy, snap frozen in isopentane cooled by liquid nitrogen, and stored at -80ºC. Phenotypic measurements were done at the time of biopsy or necropsy as previously described [41]. We evaluated 6 objective biomarkers: tibiotarsal joint (TTJ) angle, pelvic angle, TTJ tetanic flexion force (N/kg), TTJ tetanic extension force (N/kg), percent eccentric contraction decrement, and CS circumference (mm/kg) (**Figure 1**).

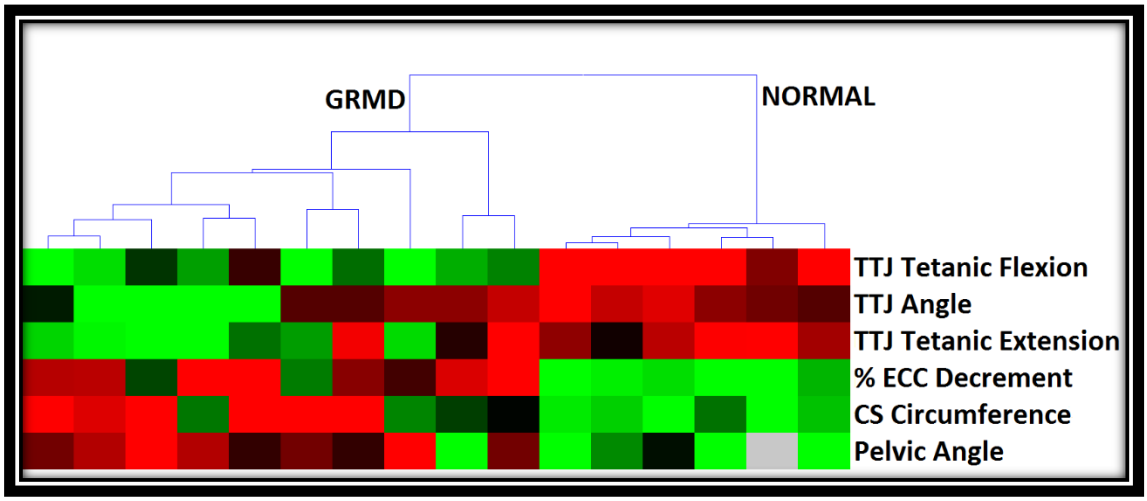

Figure 1. Heat map of unsupervised hierarchical clustering of phenotypic markers. Phenotypic measures from 6-month-old GRMD and normal dogs were visualized using unsupervised hierarchical clustering, where the color green indicates a relatively lower value for each variable and red a higher value. Distances (i.e., similarity) were based on the Pearson's correlation coefficient (r). GRMD dogs had smaller tibiotarsal joint (TTJ) angles, TTJ flexion and extension forces, and larger eccentric contraction decrements (%), CS circumferences, and pelvic angles.

2.2.2 Western Blotting

Protein lysates for Western blotting were prepared from available archived frozen (-80ºC) muscle samples, homogenized in ice cold RIPA lysis buffer (Santa Cruz Biotechnologies, #sc-24948A), stabilized with HALT™ Protease & Phosphatase inhibitor (Thermo Scientific, #78442) incubated on ice for approximately 45 minutes, and then centrifuged at 10,000 g (4°C) for 10 minutes. Pellets were discarded and supernatants for each sample were designated as crude total protein lysates. Protein lysate concentrations were estimated using the modified-Lowry method provided by the DC™ Protein Assay Kit (Bio-Rad, #5000112) [45]. Protein lysates were mixed with reducing SDS sample buffer, heated at 96°C for 5 minutes, and ~60 µg/sample were then loaded into 12% TGX Stain-Free™ polyacrylamide gels (Bio-Rad, #161-0185) for electrophoresis. The samples were run at 200V for 45 minutes in the Mini-Protean® Tetra Cell (Bio-Rad, #165-8000) to allow separation of the protein profiles. TGX Stain-free gels were imaged on the Gel Doc™ EZ System (Bio-Rad, #1708270) for activation prior to transfer using the Mini Trans-Blot® system (Bio-Rad, #170-3930). A cooled, wet transfer at 100 V for 1 hour with Tris/Glycine/0.05% SDS and 20% methanol was performed. Quality transfer of the proteins to a methanol-activated, 0.2-µm (pore size) PVDF membrane was verified using the Gel Doc™ EZ System (Bio-Rad, #1708270). After excellent protein transfer was verified, the PVDF membrane was washed with Tris-buffered saline with tween (0.1% Tween 20)(TBST) for 10 minutes, then blocked with TBST containing 5% milk for 1 hour at 20°C. Next, specific PVDF membrane pieces were washed for 10 minutes and then incubated for 1 hour at 20°C and ~17 hours

at 4°C in blocking buffer containing (1:200) APIP antibody (Thermo Fisher Scientific, #PA5-29269) with rocking. The membranes were then washed in triplicate with TBST, 10 minutes each. Membranes were subsequently probed with goat anti-rabbit HRP secondary antibody (Pierce, #31466) diluted at 1:10,000 in blocking buffer for 1 hour at 20°C. This was followed by triplicate 10-minute washes with TBST. Finally, the membranes were incubated with enhanced chemiluminescence substrate SuperSignal® West Dura (Thermo Scientific, #37071) for 5 minutes at 20°C and imaged on the Gel Doc™ XR+ System (Bio-Rad, #1708195). The cumulative chemiluminescent protocol used to collect images resulted in 60 consecutive images starting at 10 seconds and ending at 600 seconds. Images were analyzed using Image Lab™ software (Bio-Rad, Version 5.2). Protein band density was normalized by correcting for the amount of total protein loaded, estimated by measuring total lane density (LD) on the membranes. Relative fold change in protein expression was first normalized for protein loading by calculating the ratio of individual band density (i.e., APIP) and LD.

2.2.3 Immunofluorescence

Muscle samples were stored at -80ºC prior to processing. Serial muscle cryosections were cut at 7 μm for immunofluorescence. Slides were thawed, rehydrated and permeabilized in physiological buffered saline (PBS) containing 0.2% fish skin gelatin (FSG) and 0.1% Triton X-100 for 10 minutes at room temperature (~20°C), washed 2 times with PBS, fixed in cold 100% acetone for 10 minutes, washed 3 times with PBS (5 minutes each), and then blocked for 1 hour at ~20°C with 5% normal goat serum, PBS+0.3% Triton X-100. Primary antibody incubation was overnight (~17 hours)

at 4°C with the following antibodies: rabbit polyclonal APIP (Thermo Fisher Scientific, #PA5-29269, mouse monoclonal myosin heavy chain (MHC) (fast) (Leica Biosystems, #NCL-MHCf), mouse monoclonal MHC (slow) (Leica Biosystems, #NCL-MHCs), and mouse monoclonal MHC (developmental) (Leica Biosystems, #NCL-MHCd). Sections were then washed 2 times in PBS-FSG-Triton (5 minutes each) and once with PBS-FSG. Secondary antibody incubation was for 1 hour at ~20°C with goat anti-rabbit Alexa Fluor® 488 (Thermo Fisher, #A11008) and goat anti-mouse Alexa Fluor® 594 (Thermo Fisher, #A11005). Sections were washed 2 times with PBS-FSG-Triton, incubated with DAPI for 5 minutes at 20°C, and then washed 2 times with PBS-FSG-Triton and one time with PBS-FSG (5 minutes each). Sections were treated with Prolong® Gold Anti-fade reagent (Life Technologies, #P36930) and then coverslipped. Images of the sections were viewed on a Nikon Eclipse 80*i* microscope and collected for analysis with NIS-Elements Basic Research software (Laboratory Imaging, Version 3.22.14) and processing with ImageJ (National Institute of Health, Version 1.48).

2.2.4 Statistical Analysis

Data were imported into a commercial statistical software program (JMP® Pro 11.1.1.) for analysis. Median APIP protein expression levels (normalized to LD) were compared between normal vs. GRMD dogs at 6 months of age using the Wilcoxon rank-sum test ($p \leq 0.050$). Phenotypic correlations with APIP protein expression were analyzed using the conservative (non-parametric) Spearman's correlation (ρ) test ($p \leq 0.050$) because of the small sample sizes and the fact that data variation stretched the assumptions of the routine ANOVA and Pearson correlation test. The null hypothesis for

the Spearman test is that there is no association between the 2 variables (e.g., protein expression and phenotypes).

2.3 Results

2.3.1 APIP Protein Expression and Phenotypic Correlation in GRMD

Western blotting was used to establish APIP expression in the CS (n = 7 GRMD and 5 normal) and VL (n = 8 GRMD and 5 normal) muscles of 6-month-old GRMD and normal dogs. Levels did not differ (p=0.420) between normal and GRMD dogs in the hypertrophied CS **(Figure 2**). APIP expression in the CS of GRMD dogs clustered into 2 separate groups, above and below the median of the normal CS. When the single normal dog (CS) with a relatively higher APIP value was excluded from the analysis, differences in expression still did not reach significance (p=0.780).

When considering normal and GRMD dogs at 6 months, CS APIP expression correlated positively (ρ=0.6909, p=0.019) with TTJ tetanic flexion force. Although the CS is a hip flexor and does not directly contribute to TTJ flexion, its size generally correlates positively with TTJ flexion and each tracks with a more severe phenotype. In this sense, APIP expression may have contributed to a stable, hypertrophied CS phenotype but conversely been associated with an overall more severe GRMD phenotype.

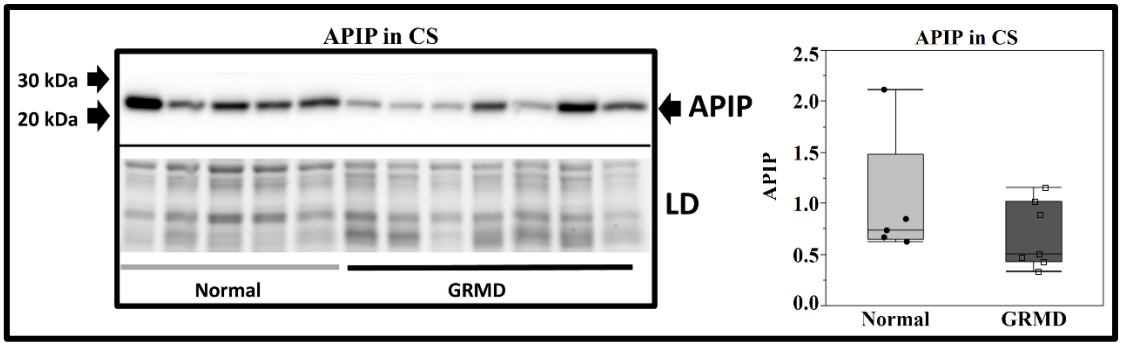

Figure 2. APIP protein expression in normal and GRMD cranial sartorius. APIP protein expression did not differ significantly between the normal and GRMD dogs. Boxplots represent the median and interquartile range. LD=Lane density.

In the VL, APIP levels were significantly higher (p=0.038) in the GRMD dogs relative to normal (**Figure 3**). As with the CS, there was notable variation among the GRMD dogs. Moreover, when including normal and GRMD dogs, VL APIP expression negatively correlated with TTJ angle (ρ= -0.7523, p=0.008). As VL APIP expression increased, the TTJ angle decreased, consistent with greater contraction and a more severe overall phenotype. Furthermore, even when considering GRMD dogs alone, VL APIP expression correlated with TTJ angle (ρ= -0.8469, p=0.016). Lower TTJ angles would be expected due to either override of stronger flexors (cranial tibialis) or weaker extensors (gastrocnemius). Importantly, while the VL does not contribute to the TTJ angle, extensor muscles generally track together. These data would suggest that APIP expression has a deleterious effect on extensor muscle strength.

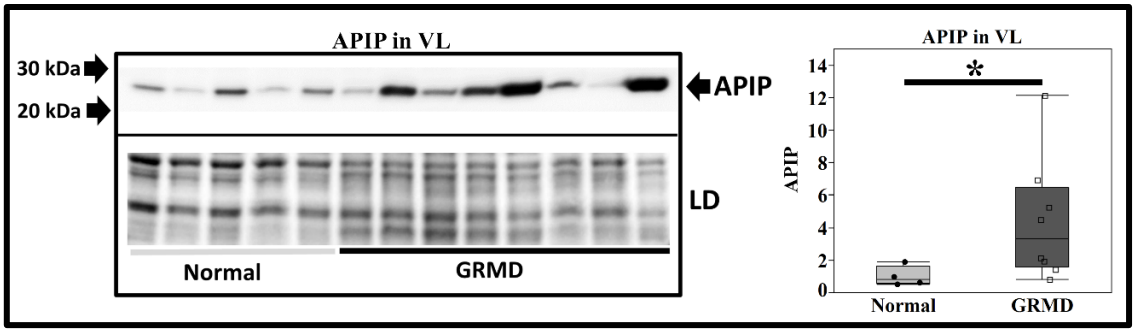

Figure 3. APIP protein expression in normal and GRMD vastus lateralis. APIP protein expression was significantly higher in the GRMD VL relative to normal dogs (*p<0.050) at 6 months of age. Box plots represent the median and interquartile range of APIP expression. LD=Lane density.

2.3.2 APIP Protein Expression Localizes To Regenerative Muscle Fibers in GRMD

Utilizing sections double-labeled with myosin heavy chain (MHC) antibodies, we demonstrated a mosaic pattern of APIP expression in both normal and GRMD muscles, suggesting fiber type specificity (**Figure 4)**.

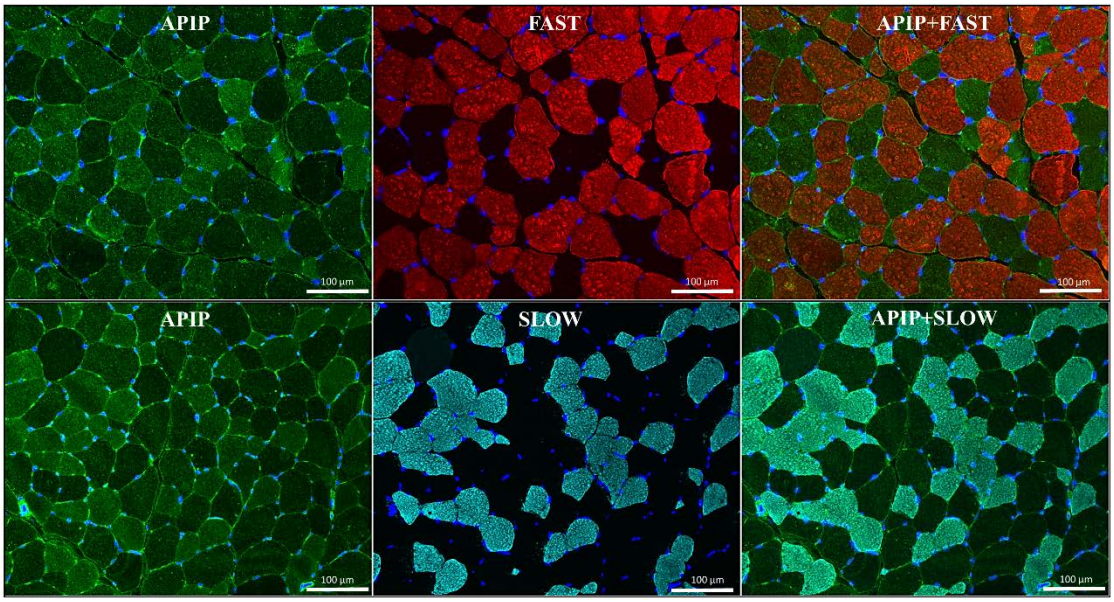

Figure 4. APIP immunofluorescence in normal canine skeletal muscle. APIP staining in normal canine cranial tibialis muscle at 6 months of age reveals a mosaic pattern indicating fiber type specificity for APIP expression. Double immunostaining for APIP (green) and MHC slow (Cyan) or fast (red) reveals that APIP is primarily expressed in slow-twitch fibers. Blue is Dapi.

Consistent with previous studies showing that anti-apoptotic factors localize primarily to regenerating fibers in damaged muscle [18, 39, 40], clusters of GRMD APIP-positive myofibers also expressed the developmental MHC isoform. Regenerative fibers often stained for both fast- and slow-MHC isoforms, in keeping with fiber type switching associated with damaged muscle (**Figure 5)**.

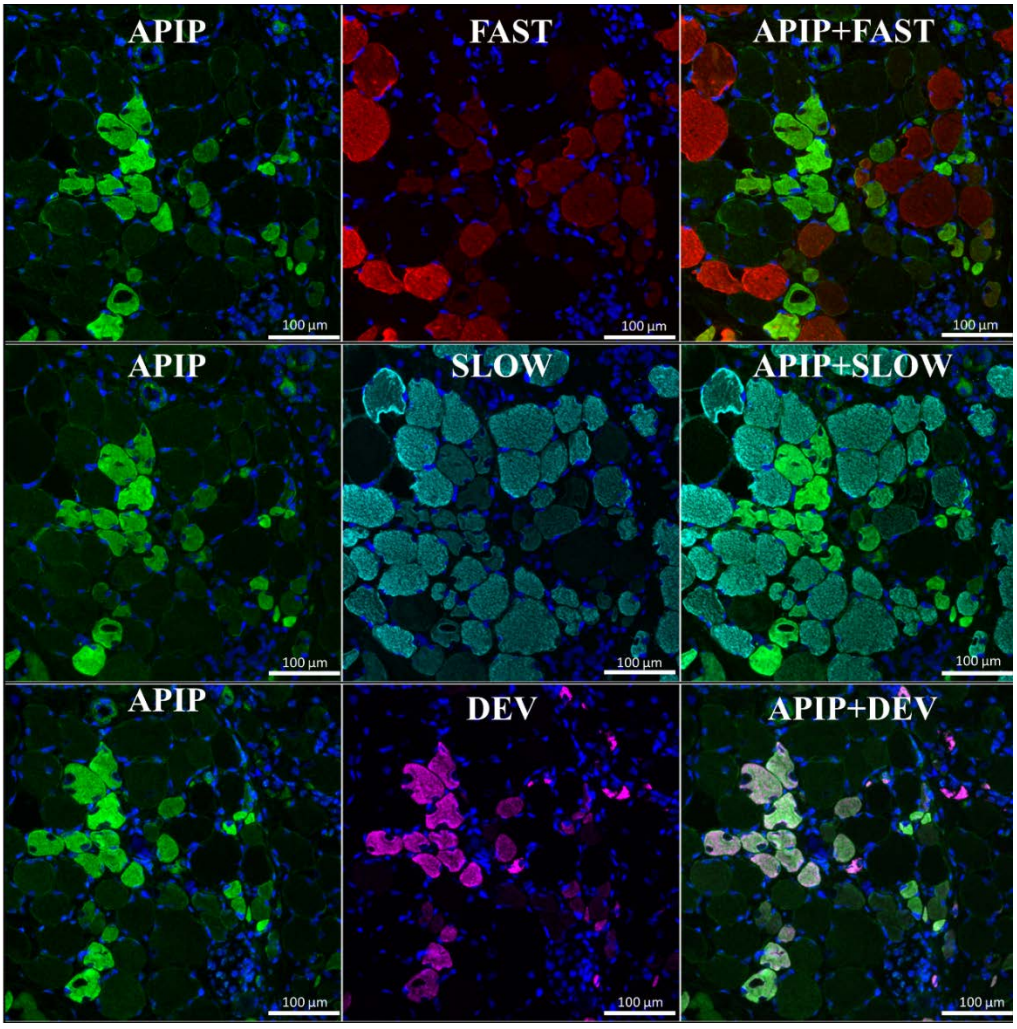

Figure 5. Immunofluorescence for APIP and MHC fiber typing in GRMD skeletal muscle. APIP co-localizes primarily with regenerating myofibers (DEV) in GRMD medial head of the gastrocnemius muscle at 6 months of age. The regenerating fibers also stain lightly for the slow- and fast- MHC isoforms consistent with fiber-type switching. Blue is Dapi.

The proportion of MHC developmental positive fibers was greater in the GRMD VL versus CS at 6 months of age (**Figure 6**), consistent with the western blot data showing APIP expression was greater in the GRMD VL. Notably, APIP was also expressed in nearby inflammatory cells in dystrophic muscle and had both cytoplasmic and membrane signals, with MHC-developmental co-localization occurring primarily with the cytoplasmic signal. (**Figure 7)**.

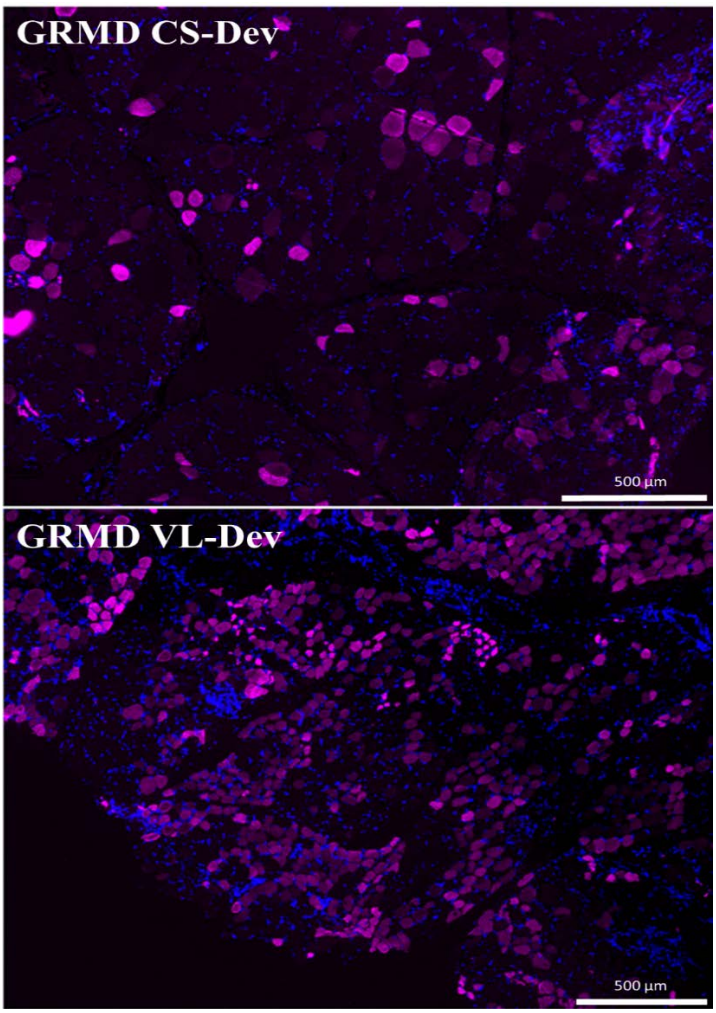

Figure 6. Immunofluorescence for MHC developmental isoform in GRMD CS and VL. Larger regenerating myofibers (magenta) in the CS express the developmental isoform of MHC, whereas the VL has a greater proportion of small, regenerative fibers.

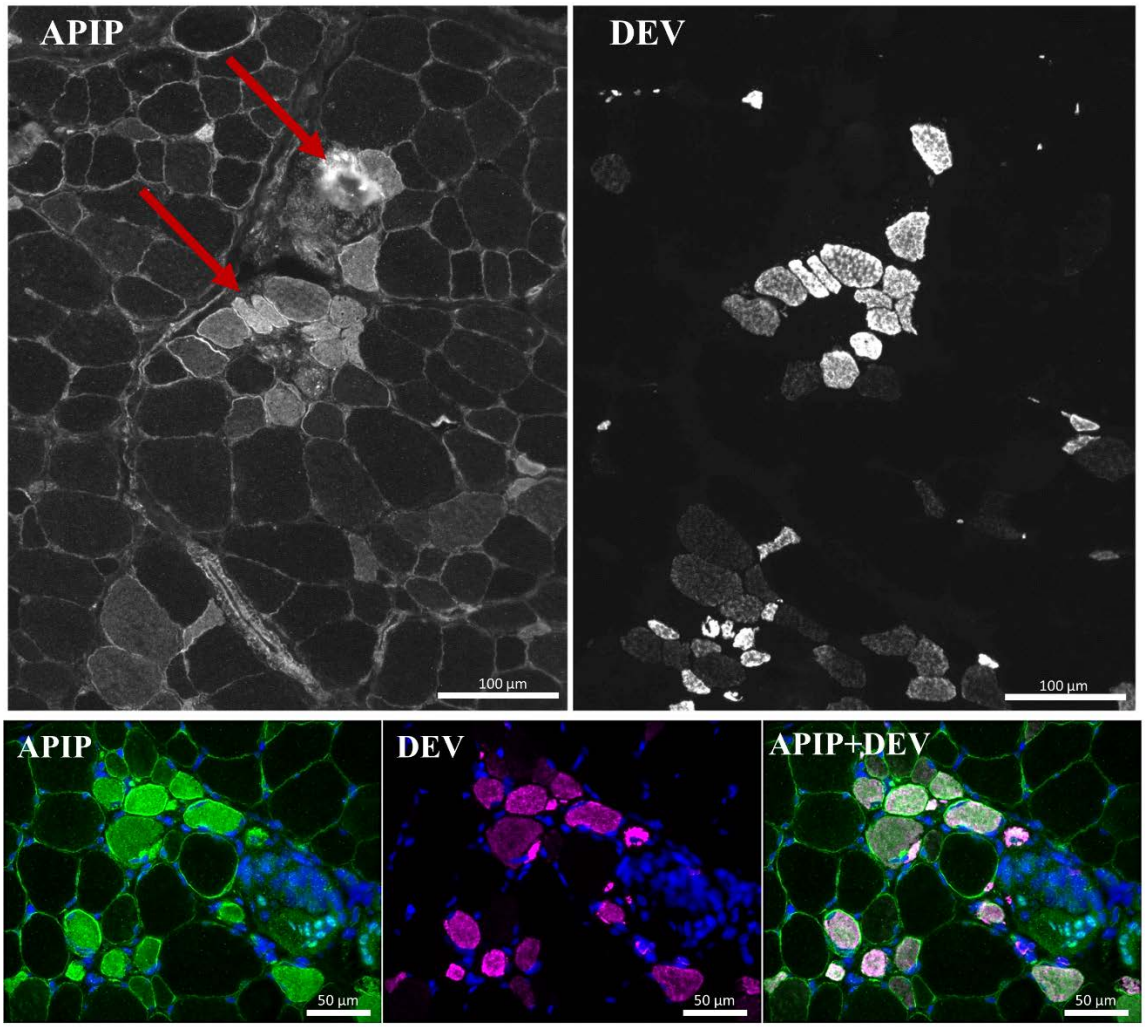

Figure 7. Immunofluorescence for APIP and MHC developmental isoform in GRMD muscle. Top Panel: In GRMD cranial tibialis muscle, APIP localizes to inflammatory cells and clusters of small myofibers that stain with MHCd (DEV), consistent with regenerating fibers. Bottom Panel: Double immunostaining confirms that cytoplasmic APIP and MHCd (DEV) co-localize, further indicating that APIP is expressed in regenerating fibers in GRMD muscle.

2.4 Discussion

This study investigated the role of APIP in GRMD pathogenesis. While not a cause of cell death in DMD, apoptosis may precede necrosis [46]. Given APIP's role in inhibiting apoptosis [35, 36], increased levels might be expected to lessen muscle injury. Indeed, inhibition of mitochondrial-associated cell death (e.g., apoptosis and necrosis)

improved the mdx mouse phenotype [19]. Interestingly, we found differential expression of APIP in the GRMD CS and VL muscles, with levels being increased over normal in the VL but not the CS. However, as opposed to an apparent beneficial effect of inhibiting cell death in the mdx mouse, increased APIP expression in the GRMD VL correlated with TTJ extensor muscle weakening and a more severe overall phenotype.

Consistent with prior studies [47, 48], we found APIP expression was fiber type specific, occurring more in slow-twitch, oxidative fibers. Importantly, for sake of our studies, the distribution of slow-twitch fibers differs between the CS (~ 51%) and superficial VL (~15%) [49]. Therefore, not surprisingly, APIP expression was greater in the normal canine CS versus VL. Furthermore, as found with other anti-apoptotic proteins, APIP was expressed primarily in regenerating myofibers in GRMD muscle [38, 39], suggesting an important role in muscle repair, over and above its specific anti-apoptotic activity. Independent of its anti-apoptotic activity, APIP is a critical enzyme in the methionine salvage pathway [50-52], which recycles 5-methylthioadenosine (MTA) produced from the polyamine synthetic process back to methionine. Accumulation of methionine salvage pathway intermediates (e.g., MTA) has been implicated in cell death and inflammation [51, 53-55]. Interestingly, APIP has also drawn considerable interest in 2 recent reports, unrelated to DMD. In one study, a dysfunctional *APIP* allele was associated with improved survival of individuals with systemic inflammatory response syndrome [50]. Conversely, in a GWAS investigating cystic fibrosis, normal functioning *APIP* tracked with more severe lung disease [56]. Our identification of APIP expression in inflammatory cells in dystrophic muscle is consistent with these findings. Mechanistic

studies, whereby APIP were up- or down-regulated and the pathological and functional effects studied, would be necessary to draw a causal association in GRMD.

In interpreting our data, it is important to distinguish between individual muscle and overall phenotype. At 6 months, the GRMD VL is characterized by active necrosis and consequently vigorous regeneration [41]. Conversely, after an early bout of necrosis, the CS has stabilized and even hypertrophied by this time. In this context, APIP could be increasing as a part of a feedback mechanism to protect cells rather than playing an active role in the injury. This study of APIP protein expression in GRMD was originally motivated by a GWAS and our subsequent discovery of its role in other diseases [52, 56, 57]. While the GRMD findings reported here further substantiate APIP as a candidate modifier gene, we have not yet done further studies necessary to substantiate this association. Other limitations of this study include the small sample size and the lack of longitudinal protein expression and methionine metabolism data. Future work should utilize targeted genome and transcriptome sequencing to determine the presence and role of variable APIP alleles and splice-variants in cell death, inflammation and methionine metabolism.

In conclusion, we have identified muscle-specific differential APIP protein expression in GRMD versus normal dogs. While we hypothesized that inhibition of apoptosis by APIP would be beneficial, VL levels tracked with a more severe phenotype. APIP was primarily expressed in slow-twitch muscle fibers of normal muscle and in regenerating fibers and inflammatory cells in dystrophic muscle. Expression in

regenerating fibers could be tied to its anti-apoptotic activity or role in methionine metabolism.

Further investigations are warranted to better define *APIP* as a candidate modifier gene and its role in muscle regeneration. Future work should include sequencing of *APIP* to search for genetic variation that could influence the biochemical properties of APIP. Additionally, future *in vivo* inquiries should evaluate other apoptotic markers (e.g., BAX, BCL2) and methionine salvage intermediates (e.g., MTA). *In vitro* experiments should also evaluate the effect of APIP expression modulation (e.g., increases or decreases) on dystrophic muscle cell growth and programmed cell death.

3. AUTOPHAGY IS DISORDERED IN GOLDEN RETRIEVER MUSCULAR DYSTROPHY

3.1 Introduction

Duchenne muscular dystrophy (DMD) is an X-linked genetic disorder, affecting approximately 1:4000 to 1:5000 live male births [1]. DMD is caused by mutations in the *DMD* gene, which results in the absence of the protein dystrophin. Dystrophin is a key component of the dystrophin-glycoprotein complex (DGC) and is critical in cell signaling and linking the muscle cytoskeleton to the extracellular matrix [2]. Without dystrophin, skeletal muscle undergoes progressive cycles of degeneration and regeneration with subsequent fibrosis, weakness, and debilitating contractures. This complex cycle of muscle damage eventually leads to wheelchair confinement, recumbence, and terminal respiratory and/or cardiovascular failure. Currently, therapies are primarily palliative in nature and often include anti-inflammatory medications (e.g., corticosteroids) and physical therapy. Corticosteroids, which are now essentially the standard of care for DMD, can only slow the destructive cyclical muscle pathology [3]. Despite discovery of the causative genetic mutation in DMD over 30 years ago, there is no cure for this fatal disease, and an urgent demand remains for development of novel therapeutics.

The 2 principal animal models used to explore novel therapeutics and perform pre-clinical studies for DMD include mdx mice and golden retriever muscular dystrophy (GRMD) dogs [4]. The pathophysiology of GRMD more closely mimics the disease

progression of DMD compared to the mildly affected mdx mice. While gene and cell-based therapies offer a potential cure and are being pursued in animal models (e.g., mouse and canine) and DMD clinical trials, there is also considerable interest in reducing the so-called secondary effects of dystrophin loss. Identification of therapeutics that could lessen fibrosis, inflammation, and accumulation of damaged proteins and organelles, without the side effects of corticosteroids, remains an important objective in DMD research. Recently, macroautophagy (hereafter known as autophagy) has been implicated as a novel therapeutic target in various muscular dystrophies, including DMD [27].

Autophagy is a conserved biological mechanism essential for survival of eukaryotic cells that involves organized degradation ("self-eating)" and recycling of cellular building blocks into macromolecules [21]. The tagged cytoplasmic contents (e.g., damaged proteins and organelles) are captured and carefully enclosed into the autophagosome, which then binds to the lysosome forming the autolysosome. Lysosomal hydrolases convert the cargo to macromolecules for re-use by the cell. In addition to cleaning up cellular "garbage," autophagy removes damaged mitochondria to ensure they do not contribute to excessive oxidative stress [22]. This multi-step cellular process requires a functional lysosomal system and coordination of over 30 different proteins [24]. Dysregulation at any of these steps can affect tissue homeostasis and contribute to disease.

Post-mitotic cells (e.g., myofibers and neurons) are more susceptible to disruptions in autophagy and subsequent accumulation of excessive damaged/toxic

proteins and organelles and cellular senescence [25]. Tight regulation of autophagy is critical for maintaining homeostasis in skeletal muscle, with either too much or too little resulting in muscle atrophy and cell death [27, 28]. Data from primarily *mdx* mice have shown a reduction in autophagic flux, with reduced autophagosomes and increased p62 accumulation, suggesting that autophagy is dysregulated in dystrophin-deficient skeletal muscle [58-64]. Progressive accumulation of damaged proteins and mitochondria would logically be injurious and compound the insult to dystrophin deficient muscle cells [58-64] . The exact cause for this dysregulation is likely multi-factorial, with several proposed contributing factors, including Akt activation (inhibits autophagy through forkhead box O [FoxO]) and excessive oxidative stress (inhibits autophagy through Src-kinase) [58, 62, 65-67]. Some insight on underlying pathogenic mechanisms has been gained by treatment strategies that have consistently improved the mdx phenotype [58-60, 62, 63].

Considering the paucity of literature regarding autophagy in DMD and that the GRMD phenotype better mimics that of DMD, we sought to investigate autophagy in phenotypically distinct skeletal muscles from age-matched dystrophic and normal dogs. A multi-modal approach, including gene and protein expression followed by light and transmission electron microscopy, was used. We hypothesized that autophagy would be dysregulated in GRMD skeletal muscle and, more specifically, that autophagic activity would be reduced, with an associated increase in damaged proteins and organelles. Additionally, we hypothesized that dysregulation of autophagy would correlate with phenotype of both the individual dog and variably affected muscle. In this report, we

demonstrate that autophagy is impaired in the skeletal muscle of GRMD dogs and this dysregulation correlates with phenotype and varies between muscle types. In particular, disordered autophagy in the GRMD cranial sartorius muscle appears to contribute to the classical true hypertrophy seen in this muscle.

3.2 Materials and Methods

3.2.1 Animals

Dogs were from a colony at the University of North Carolina at Chapel Hill (UNC-CH) that was subsequently moved to Texas A&M University (TAMU). They were cared for and assessed according to principles outlined in the National Research Council Guide for the Care and Use of Laboratory Animals. Studies were approved by the UNC-CH Institutional Animal Care and Use Committee (IACUC) through protocol, Natural History and Immunological Parameters in the German Shorthaired Pointer Muscular Dystrophy (GSHPMD) (09-011). Overall care and biomarkers used to characterize phenotype were covered by IACUC protocol, Standard Operating Procedures—Canine X-Linked Muscular Dystrophy (09-351). The GRMD dystrophic genotype was originally suspected in newborn pups based on elevated serum creatine kinase (CK) and confirmed by polymerase chain reaction (PCR), as previously described [5].

The study included untreated GRMD dogs and age-matched wild type littermates. Sample numbers varied between comparisons depending on tissue availability. Comparative longevity studies for dogs and humans indicate that the first

year of a golden retriever's life roughly equates to 20 years of a human [68]. In this context, a parallel can be drawn between the relatively rapid disease progression seen at 3-6 months in GRMD and 5-10 years in DMD. For sake of GRMD preclinical trials, we typically establish baseline data, including analysis of muscle biopsies, before beginning treatment at 3 months and collect the same outcome data at 6 months. In keeping with this approach, muscle samples were collected by biopsy at 3 months of age from the cranial sartorius (CS) and vastus lateralis (VL) muscles and at 6 months by biopsy or necropsy from the contralateral CS, VL, cranial tibialis (CT), medial head of the gastrocnemius (MHG), and diaphragm. These muscles and ages were collected based on their clear differential involvement at 3 and 6 months of age [42, 43]. For example, at 3 months the CS has already undergone a period of necrosis, while the VL remains mildly affected. However, by 6 months of age, the CS has hypertrophied, while the VL shows greater necrosis due to its role in weight bearing [11, 43]. Furthermore, for sake of functional studies, our previous work has shown that results best correlate at 6 months [41].

For all studies, samples were snap frozen in isopentane, cooled by liquid nitrogen, and stored at -80ºC for future analysis. A total of 8 objective biomarkers (tibiotarsal joint [TTJ] angle; pelvic angle; maximum hip flexion angle; maximum hip extension angle; TTJ tetanic flexion force; TTJ tetanic extension force; percent eccentric contraction decrement; and, CS circumference) were assessed at the time of biopsy or necropsy as previously described [41].

3.2.2 RNA Extraction and Gene Expression

Total mRNA expression was estimated in skeletal muscles (**Table 1)** using quantitative real-time PCR (qPCR) for the following genes: *MAP1LC3B*, *ATG12*, *BCN1*, *BNIP3*, *FBXO32*, *TRIM63*, and *HPRT1*. Total cellular ribonucleic acid (RNA) was isolated from frozen skeletal muscle samples utilizing TriPure Isolation Reagent (Roche, #11667157001) and tissue homogenization. Total RNA samples were DNase treated with Ambion Deoxyribonucleic Acid (DNA)-*free* kit™ (Applied Biosystems, #AM1906). RNA concentrations of the individual samples were measured using a Nanodrop 2000 spectrophotometer. RNA quality was assessed using a 2100 BioAnalyzer (Agilent Technologies) and all samples had a RIN>9. Samples of skeletal muscle RNA (100 ng) were reverse transcribed into cDNA using oligo-dT, random octamer primers and the SuperScript® II Reverse Transcription Kit (Invitrogen, #18064-014). Primers were designed using the NCBI Primer-Blast tool to target spanning exons for 4 autophagy genes (*MAP1LC3B*, *ATG12*, *BCN1*, and *BNIP3*), 2 ubiquitin-proteasome system (UPS) genes (*FBXO32*, *TRIM63*) and 1 housekeeping gene (*HPRT1*)(**Table 2)**. PCR primer efficiency was estimated using the LinRegPCR program (Version 2015.3) to ensure the primer pair amplification factor was >1.9 [69-71]. The qPCR was performed in triplicate reactions with Power SYBR® Green PCR Master Mix (Applied Biosystems, #4367659) on an Applied Biosystems 7900HY Fast Real-Time PCR System. Relative fold changes in gene expression between normal and GRMD muscles were calculated using the comparative C(T) method and the equation $2^{-\Delta Ct}$ with *HPRT1* as the house keeping gene [72].

Table 1. Sample sizes for gene expression.

Muscle	Age (months)	Normal (n=)	GRMD (n=)
CS	3	6	10
VL	3	8	11
CS	6	6	11
VL	6	4	10
CT	6	4	5
MHG	6	4	5
Diaphragm	6	3	4

Table 2. Primers for qPCR.

Gene Name	Forward Primer	Reverse Primer
MAP1LC3B	TTCAAGCAGCGTCGCACCTT	GCTGTAAGCGCCTCCTAATGAT
ATG12	CCCGAACCATTCAAGGACTCA	CCCAGAGCTGTTTCCTTTGT
BCN1	TCAGGAGGAAGCTCAGTATCAGA	TGTGCCGAACTGTCCACTGT
BNIP3	AGCTCCCAGTCTGAGGAAGA	TTCCGGCCGACTTGACCAAT
FBXO32	TGACGTTGCAGCCAAGAAGA	CAGTTCCAACAGCCGCACAA
TRIM63	TGCTCCATGTGCAAGGTGTT	TGACTGTTCTCCTTGGTCACT
HPRT1	AGCTTGCTGGTGAAAAGGAC	TTATAGTCAAGGGCATATCC

3.2.3 Western Blotting

Protein expression of the autophagosome marker LC3B-II and the autophagy readout protein p62/SQSTM1 were evaluated in the CS (n=5 normal and 7 GRMD) and VL (n=5 normal and n=8 GRMD) of 6-month-old dogs using Western blotting [24]. To prepare protein lysates, frozen muscle samples were homogenized in RIPA lysis buffer (Santa Cruz Biotechnologies, #sc-24948A) and stabilized with HALT™ Protease & Phosphatase inhibitor (Thermo Scientific, #78442). Samples were incubated on ice for approximately 45 minutes and then centrifuged at 10,000 g (4°C) for 10 minutes. Pellets were discarded and supernatants for each sample were designated as the crude total protein lysates. Protein lysate concentrations were estimated using the modified-Lowry method provided by the DC™ Protein Assay Kit (Bio-Rad, #5000112) [45]. Protein

lysates were mixed with reducing SDS sample buffer, heated at 96°C for 5 minutes, than ~60 µg/sample were loaded into 12% TGX Stain-Free™ polyacrylamide gels (Bio-Rad, #161-0185) for electrophoresis. The samples were run at 200 V for 45 minutes in the Mini-Protean® Tetra Cell (Bio-Rad, #165-8000) to allow for adequate separation of the protein profiles. To activate the TGX Stain-free gels prior to transfer, they were imaged on the Gel Doc™ EZ System (Bio-Rad, #1708270). Protein transfer was performed using the Mini Trans-Blot® system (Bio-Rad, #170-3930). A cooled, wet transfer at 100V for 1 hour with Tris/Glycine/0.05% SDS and 20% methanol was performed. Quality transfer of the proteins to a methanol-activated, 0.2-µm (pore size) PVDF membrane was verified using the Gel Doc™ EZ System (Bio-Rad, #1708270). After excellent protein transfer was verified, the PVDF membrane was cut into 2 pieces (>20 kDa and <20 kDa), which allowed for simultaneous probing for 2 autophagy-related proteins (LC3B and p62) of different molecular weights. The membrane was washed with Tris-buffered saline with 0.1% Tween 20 (TBST) for 10 minutes, then blocked with TBST containing 5% milk and 1% BSA for 1 hour at 20°C. Next, specific PVDF membrane pieces were washed for 10 minutes and then incubated for 1 hour at 20°C and ~17 hours at 4°C in blocking buffer containing LC3B antibody (Novus Biologicals, #NB100-2220) or p62/SQSTM1 antibody (Novus Biologicals, #NBP1-49954) with rocking. The membranes were then washed in triplicate with TBST, 10 minutes each. Membranes were subsequently probed with goat anti-rabbit HRP secondary antibody (Pierce, #31466) diluted at 1:10,000 in blocking buffer for 1 hour at 20°C. This was followed by triplicate 10-minute washes with TBST. Finally, the membranes were

incubated with enhanced chemiluminescence substrate SuperSignal® West Dura (Thermo Scientific, #37071) for 5 minutes at 20°C and imaged on the Gel Doc™ XR+ System (Bio-Rad, #1708195). A cumulative chemiluminescent protocol was used to collect 60 consecutive images starting at 10 seconds and ending at 600 seconds. The images were analyzed using the Image Lab™ software (Bio-Rad, Version 5.2). Normalization of band density for the protein of interest was performed by correcting for the amount of total protein loaded. This was estimated by measuring the total regional lane density identified on the PVDF membranes. Relative fold change in protein expression was normalized for protein loading by calculating the ratio of individual band density (e.g., LC3B-II, p62) and total lane density (LD).

3.2.4 Light Microscopy

Muscle samples were stored at -80ºC prior to processing. Serial muscle cryosections were cut at 7 μm and stained with hematoxylin and eosin (H&E) and modified-Gomori Trichrome for histopathologic assessment. For immunofluorescence, serial cryosections were thawed, rehydrated and permeabilized in physiological buffered saline (PBS) containing 0.2% fish skin gelatin (FSG) and 0.1% Triton X-100 for 10 minutes at room temperature (~20°C) and then washed 2 times with PBS. Sections were then fixed in cold 100% acetone for 10 minutes and then washed 3 times with PBS (5 minutes each). Sections were blocked for 1 hour at ~20°C with 5% normal goat serum, PBS+0.3% Triton X-100. Primary antibody incubation was overnight (~17 hours) at 4°C with the following antibodies: rabbit monoclonal LC3B (D11) XP® (Cell Signaling, #3868), mouse monoclonal myosin heavy chain (fast) (Leica Biosystems, #NCL-MHCf)

and mouse monoclonal myosin heavy chain (slow) (Leica Biosystems, #NCL-MHCs). Sections were then washed 2 times in PBS-FSG-Triton (5 minutes each) and then once with PBS-FSG. Secondary antibody incubation was for 1 hour at ~20°C with the following antibodies: goat anti-rabbit Alexa Fluor® 488 (Thermo Fisher, #A11008) and goat anti-mouse Alexa Fluor® 594 (Thermo Fisher, #A11005). Sections were washed 2 times with PBS-FSG-Triton and then incubated with DAPI for 5 minutes at 20°C. Sections were washed 2 times with PBS-FSG-Triton and once with PBS-FSG (5 minutes each). Prolong® Gold Anti-fade reagent (Life Technologies, #P36930) was placed on the sections followed by coverslips. Images of the sections were viewed on a Nikon Eclipse 80*i* microscope and collected for analysis with NIS-Elements Basic Research software (Laboratory Imaging, Version 3.22.14). Further imaging processing was performed in ImageJ (National Institute of Health, Version 1.48).

3.2.5 Transmission Electron Microscopy

To define autophagosomes morphologically, CS and VL muscle samples were collected at necropsy from 6-month-old GRMD dogs (n=4) and routinely prepared for transmission electron microscopy (TEM). Autophagosomes were defined as vesicular compartments with double-limiting membranes containing heterogeneous cytosolic materials or mitochondria [73]. Muscle samples were fixed immediately in 3% glutaraldehyde + 2% paraformaldehyde buffered with 0.1 M sodium cacodylate (pH 7.4) for 1 hour. Individual muscle fascicles were dissected from each muscle sample and placed in fresh fixative overnight at 4°C. Muscle fascicles were then removed from the fixative and washed with 0.1 M sodium cacodylate solution. Following fixation, tissues

were treated with 2% OsO_4+1.5% K Ferrocyanide in 0.1 M sodium cacodylate for 5 hours at room temperature. Next, tissues were washed 3 times with H_2O for 5 minutes each and then incubated with 2% uranyl acetate (UA) in distilled water for 3 hours. Following UA treatment, the tissue was washed overnight in H_2O at room temperature and 3 times with H_2O prior to dehydration. Tissues were dehydrated using a graded series of absolute EtOH solutions finishing with absolute acetone and then incubated overnight with 1/3 EMbed 812 Resin (EMS, #812) and 2/3 absolute acetone at room temperature. Next, samples were incubated with 2/3 Resin and 1/3 absolute acetone at room temperature for 8 hours and then overnight in 100% Resin. Finally, tissues were placed in molds, embedded in resin and baked at 60ºC for ~72 hours. Thin sections (80 nm) were placed on formvar-coated mesh grids and copper mesh grids for staining with UA and lead citrate. Images were collected from an FEI Transmission Electron Microscope in the Image Analysis Laboratory at Texas A&M University and digitally captured for analysis.

3.2.6 Statistical Analysis

All values are expressed as means ± 95 % confidence interval. Statistical differences in gene and protein expression between different muscles of normal and GRMD dogs were analyzed using a one-way ANOVA ($p<0.05$). Phenotypic correlations with gene and protein expression were analyzed with the Spearman's correlation test ($p<0.05$). We chose this conservative route because of the small sample sizes and the fact that data variation stretched the assumptions of the Pearson correlation test. The null hypothesis for the Spearman test is that there is no association between the 2 variables

(e.g., gene or protein expression and phenotypes). All analyses and graphs were created with JMP® Pro 11.1.1.

3.3 Results

3.3.1 Gene Expression in Muscles of Normal and GRMD Dogs

A total of 4 autophagy-related genes (*MAP1LC3B, ATG12, BCN1,* and *BNIP3)* and 2 ubiquitin proteasome system (UPS) genes (*FBXO32, TRIM63*) were analyzed. We were particularly interested in *MAP1LC3B* gene expression since it is essential for autophagosome biogenesis [74]. Expression was lower in the GRMD versus normal CS at both 3 and 6 months of age (**Figure 8A**) and in the VL at 3 but not 6 months. *MAP1LC3B* levels also trended towards lower levels in the CT, MHG, VL, and diaphragm at 6 months.

The *ATG12* gene codes for ATG12, which is a component of the ATG12-ATG5-ATG16 protein conjugation complex essential for autophagy [75]. *ATG12* expression was lower in the CS only at 3 months (p=0.036) with a trend at 6 months (**Figure 8B**). Interestingly, *ATG12* levels were higher in the GRMD MHG (p=0.033) at 6 months of age compared to normal dogs. In further contrast to the GRMD CS at 6 months, the VL (p=0.074) and diaphragm (p=0.052) also trended towards being higher compared to normal dogs.

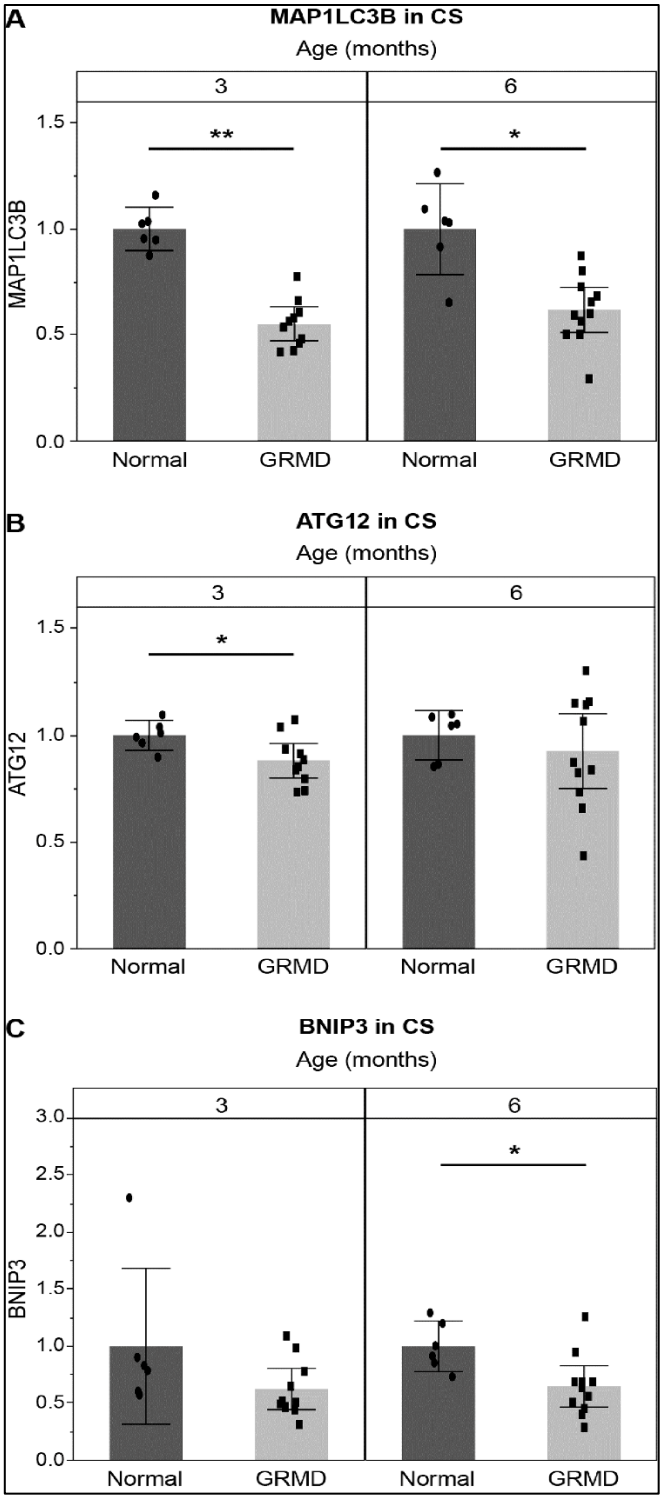

Figure 8. Autophagy gene expression in the cranial sartorius. A) MAP1LC3B gene expression was lower at 3 and 6 months of age in GRMD dogs. B) ATG12 expression was lower in 3-month-old GRMD dogs. C) BNIP3 was lower in 6-month-old GRMD dogs. Bar graphs represent mean expression +/- 95 % confidence interval. *p<0.050, **p<0.010.

BCN1 codes for the Beclin 1 protein, which is novel regulator of autophagy induction and involved in autophagosome biogenesis (i.e., initiation and nucleation)[76]. While levels in GRMD and normal dogs did not differ for any muscle at either 3 or 6 months of age, there was a trend towards higher values in GRMD. This difference neared significance in the VL at 3 months (p=0.078) and in the MHG at 6 months (p=0.073).

BNIP3 codes for the Bnip3 protein, which is a potent inducer of autophagy and critical for selective autophagy of mitochondria and the endoplasmic reticulum [77]. *BNIP3* levels were generally lower in GRMD muscles at both 3 and 6 months of age, with the most significant differences being in the 3-month VL (p=0.001) and 6 month CS (p=0.015) (**Figure 8C)**.

We also assessed expression of 2 genes (*FBXO32, TRIM63*) that code for ubiquitin ligases, which directly track with UPS activation and are essential for muscle atrophy [78]. Both were significantly lower in the CS at 3 months (*FBXO32*, p=0.010; TRIM63, p=0.001). In the 6 month samples, *TRIM63* was higher in the diaphragm (p=0.039), while levels appeared to be normalizing in the CS.

In summary, gene expression in GRMD muscles at both 3 and 6 months of age was generally compatible with down-regulation of autophagy signaling without significant activation of the UPS. Findings from the CS at 6 months were most remarkable, with significant down-regulation of both *MAP1LC3B* and *BNIP3.* It is not surprising that *MAP1LC3B, ATG12,* and *BNIP3* tracked together, because FOXO3 has

been shown to be a master regulator of several autophagy-related genes in skeletal muscle [67].

3.3.2 Autophagy Gene Expression Correlates with GRMD Phenotype

The dystrophinopathies demonstrate dramatic phenotypic variation at several levels, including muscle (e.g., CS vs. VL), individual dystrophic humans or dogs, and species (e.g., mdx vs GRMD). This phenotypic variation provides a platform to better understand pathophysiologic mechanisms and genetic modifiers. In principle, meaningful molecular changes should track with phenotype. With that said, such an association does not necessarily prove cause and effect.

BNIP3 in the CS correlated positively with TTJ tetanic flexion (N/kg) when assessing all GRMD and normal dogs, or GRMD dogs alone (**Table 3**). Even though the CS does not act on the TTJ joint, CS circumference and TTJ tetanic force correlate directly. Thus, this correlation provided indirect evidence of a causal association. With a more direct functional comparison, expression of CS *MAP1LC3B* in all dogs and *BCN1* in GRMD dogs alone correlated negatively with CS circumference. Considering the critical role Beclin 1 plays in autophagy induction and autophagosome biogenesis, identifying a negative correlation with CS circumference suggests that reduced autophagy could contribute to CS hypertrophy, which tends to track with a more severe GRMD phenotype [43, 76].

BNIP3 VL expression and tetanic TTJ flexion correlated positively at 6 months when assessing both GRMD and normal dogs (Spearman ρ=0.6703, p=0.012) or GRMD

dogs alone (**Table 3**). As with the CS, VL *BCN1* expression correlated negatively with CS circumference, suggesting that the CS finding could be nonspecific.

Table 3. Autophagy gene expression at 6 months of age correlates with phenotype.

Genotype	Muscle	Variable	by Variable	Spearman ρ	Prob >|ρ|
Normal & GRMD	CS	CS Circumference (MM/KG)	*MAP1LC3B*	-0.7206	0.002
Normal & GRMD	CS	TTJ Tetanic Flexion (N/KG)	*MAP1LC3B*	0.6618	0.005
Normal & GRMD	CS	Pelvic Angle (º)	*MAP1LC3B*	-0.6361	0.011
Normal & GRMD	CS	TTJ Angle (º)	*MAP1LC3B*	0.5093	0.044
Normal & GRMD	CS	TTJ Tetanic Flexion (N/KG)	*BNIP3*	0.7647	0.001
Normal & GRMD	CS	TTJ Tetanic Extension (N/KG)	*BNIP3*	0.7118	0.002
Normal & GRMD	CS	TTJ Angle (º)	*BNIP3*	0.6159	0.011
GRMD	CS	CS Circumference (MM/KG)	*BCN1*	-0.6848	0.029
GRMD	CS	TTJ Tetanic Flexion (N/KG)	*BNIP3*	0.7455	0.013
GRMD	CS	Hip Flexion Angle (º)	*FBXO32*	0.6862	0.041
GRMD	CS	TTJ Tetanic Extension (N/KG)	*TRIM63*	-0.8424	0.002
GRMD	CS	Pelvic Angle (º)	*TRIM63*	0.7841	0.007
GRMD	VL	CS Circumference (MM/KG)	*BCN1*	-0.8167	0.007
GRMD	VL	TTJ Tetanic Flexion (N/KG)	*BNIP3*	0.7167	0.030
GRMD	VL	TTJ Tetanic Flexion (N/KG)	*FBXO32*	0.7143	0.046
GRMD	VL	TTJ Tetanic Extension (N/KG)	*FBXO32*	0.7143	0.046
Normal & GRMD	MHG	TTJ Tetanic Flexion (N/KG)	*BCN1*	-0.8	0.010
Normal & GRMD	MHG	TTJ Tetanic Flexion (N/KG)	*ATG12*	-0.7833	0.012
Normal & GRMD	MHG	TTJ Angle (º)	*ATG12*	-0.7596	0.018
Normal & GRMD	MHG	CS Circumference (MM/KG)	*ATG12*	0.6667	0.049
GRMD	MHG	Hip Extension Angle (º)	*BCN1*	-1	<0.001
GRMD	MHG	Pelvic Angle (º)	*FBXO32*	0.9747	0.005
GRMD	MHG	TTJ Tetanic Extension (N/KG)	*MAP1LC3B*	-0.9	0.037
GRMD	MHG	TTJ Tetanic Extension (N/KG)	*FBXO32*	-0.9	0.037
GRMD	MHG	CS Circumference (MM/KG)	*TRIM63*	0.9	0.037
GRMD	MHG	Hip Flexion Angle (º)	*MAP1LC3B*	0.9	0.037
GRMD	MHG	Hip Flexion Angle (º)	*FBXO32*	0.9	0.037

The CT contributes to TTJ flexion so correlations here could be particularly meaningful. *MAP1LC3B* expression in GRMD dogs considered alone correlated negatively with TTJ tetanic flexion force (Spearman ρ=-0.9, p=0.037), consistent with autophagy having a degradative role. Otherwise, *BNIP3* expression correlated positively with maximum hip extension angle of both the grouped GRMD and normal dogs

(Spearman ρ=0.8667, p=0.002) and GRMD dogs alone (Spearman ρ=0.9, p=0.037). A degradative effect on hip flexors analogous to that seen in the CT could, in principle, expand hip extension. However, as discussed above, CS *MAP1LC3B* and BCNI expression correlated negatively with CS circumference, suggesting that down-regulation of autophagy genes might actually contribute to CS hypertrophy.

The MGH contributes to TTJ extension; therefore, correlations are likely to be meaningful. To this effect, *MAP1LC3B* and *FBXO32* in GRMD dogs alone correlated negatively with TTJ tetanic extension force (**Table 3**). Increased autophagy would potentially enhance muscle degradation, thus accounting for the negative correlation. The functional relationship between ATG12 and TTJ angle could have a similar explanation. Increased degradation and associated weakening of the MGH would allow TTJ flexors to predominate and lessen the angle. Other correlations between MHG gene expression and TTJ flexion and CS circumference are likely not consequential, given that the MGH does not play a role in either test.

In summary, of the genes studied, *MAP1LC3B* appeared to have the most consequential role in GRMD disease expression. As discussed earlier, levels were lower in the GRMD CS at 3 and, to a lesser extent, 6 months of age. Lower *MAP1LC3B* at 3 months would logically have greater consequential effects on functional data at 6 months, when persistently lower values correlated with CS circumference. This suggests that reduced CS autophagy could contribute to the classical true hypertrophy seen in this muscle [11, 43]. Gene expression was only studied in the CT and MGH muscles at age 6 months, at which time there was only a trend towards lower GRMD expression.

Assuming a similar age effect to that seen in the CS, *MAP1LC3B* would be expected to be even more down-regulated in these muscles at 3 months. Thus, just as with the CS, the negative correlation between *MAP1LC3B* levels and TTJ tetanic flexion force would be in keeping with a role for reduced autophagy in the functional hypertrophy seen in TTJ flexors at age 6 months [42]. A similar negative correlation was seen between *MAP1LC3B* expression and TTJ tetanic extension force at age 6 months. As opposed to hypertrophy seen in TTJ flexors at 6 months, TTJ extensors such as the MGH are atrophied and weaker [42, 43]. This points to the complexity and diversity of the regulatory systems among different muscles. Activation or inhibition of autophagy may be beneficial in one muscle and deleterious in another.

3.3.3 Autophagy Protein Expression in Muscles of Normal and GRMD Dogs

Gene expression does not necessarily track with protein levels and activity. To better establish overall autophagic activity, we used Western blotting to assess the established autophagosome marker LC3B-II and the autophagy readout protein p62/SQSTM1 [24]. LC3B-II levels in the GRMD CS were increased over normal, with a mean fold change of 9.03 ($p=0.014$) **(Figure 9**), indicating accumulation of autophagosomes in a range of potential cells (satellite cells, myocytes, fibroblasts, immune cells, adipocytes and blood vessels) due to either increased flux, decreased clearance, or an overwhelmed autophagic system.

We then assessed expression of p62, a readout protein relatively specific for autophagic activity. If autophagic flux were increased in the dystrophic CS, p62 levels should be lower. Interestingly, 3 distinct p62 bands were identified in the CS samples.

These different bands could represent different isoforms, off target antibody binding or post-translation modifications of p62. Levels of the intermediate 60 kDa band were significantly higher in GRMD dogs (Fold Change = 5.25, p=0.004) (**Figure 9**), consistent with decreased autophagic flux.

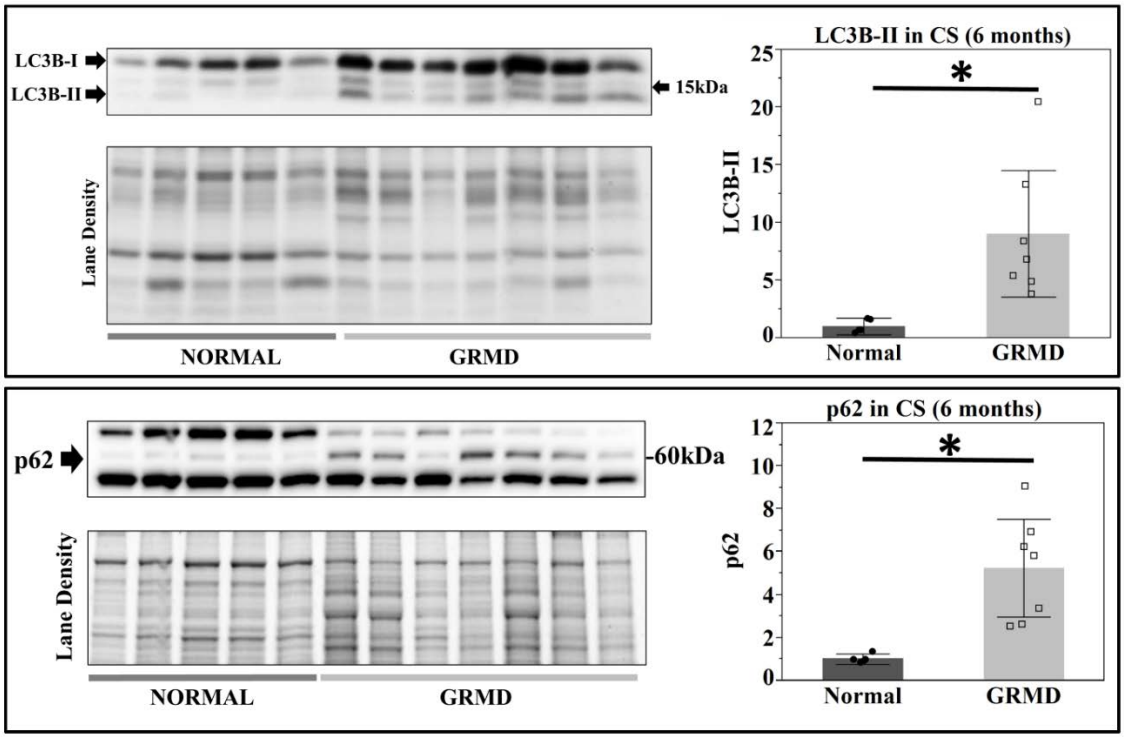

Figure 9. Western blots for LC3B and p62 in the CS of 6-month-old normal and GRMD. LC3B-II and p62 were significantly higher in the GRMD CS at 6 months of age relative to normal dogs. Bar graphs represent mean +/- 95% confidence interval. *p<0.05.

With normal balanced autophagy, increased LCB-II activity should track with decreased p62 expression. The lack of such a balance suggests that autophagy may be dysregulated in the GRMD CS muscle. As discussed earlier, the CS undergoes early necrosis and then stabilizes and may even hypertrophy. We next repeated these studies

in the VL, which has a more delayed onset of active necrosis and is typically atrophied at 6 months. Mean LC3B-II expression was higher in the VL of GRMD versus normal dogs (Fold Change = 2.35) but the difference was not significant (p=0.140) (**Figure 10**). However, p62 was significantly increased in the GRMD VL relative to normal dogs (Fold Change = 4.7, p=0.042) (**Figure 10**). Taken together, these findings suggest that autophagic activity is decreased in the GRMD VL at age 6 months.

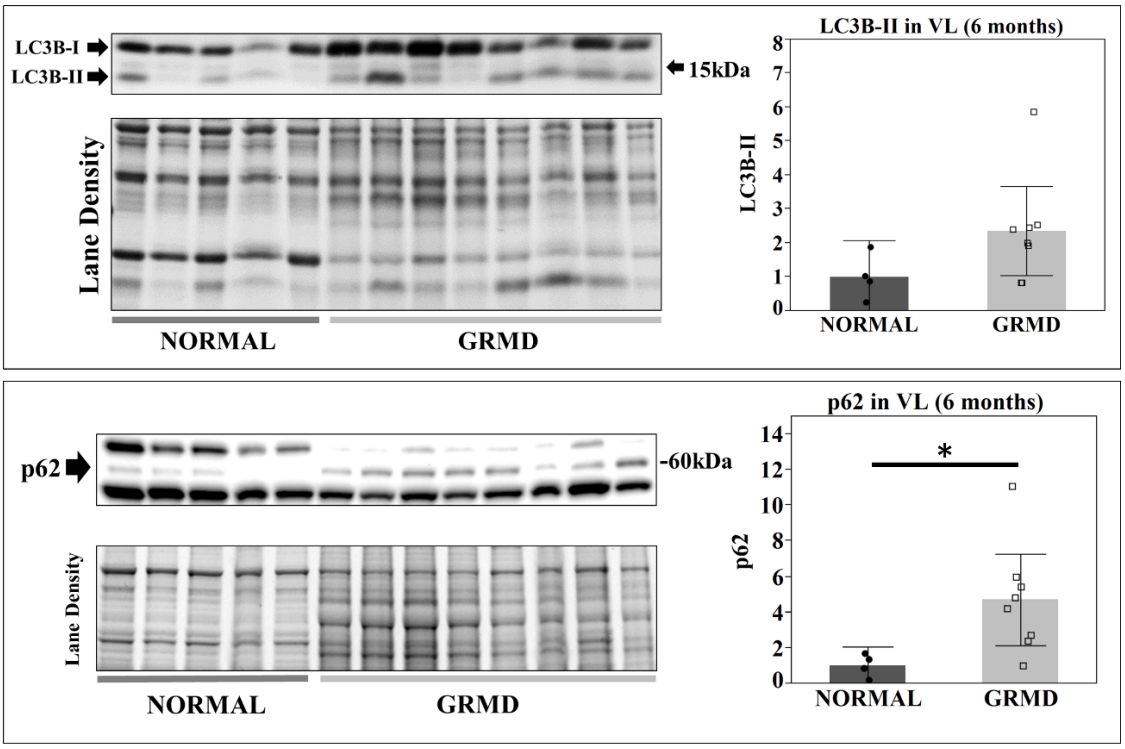

Figure 10. Western blots for LC3B and p62 in the VL of 6-month-old normal and GRMD dogs. LC3B-II was not significantly higher in the GRMD VL relative to normal. However, p62 was significantly higher in GRMD VL. Bar graphs represent the mean +/- 95% confidence interval. *p<0.050.

3.3.4 Autophagy Protein Expression Correlates with Phenotype in GRMD

Protein expression data were correlated with functional test results to infer potential clinical significance. Starting with the CS, LC3B-II and p62 activity correlated positively with CS circumference, drawing an association between impaired autophagosome clearance and hypertrophy. Impaired autophagic activity could contribute to the disordered repair response that allows muscle hypertrophy to occur. Turning to GRMD dogs considered alone, p62 levels in the CS correlated positively with pelvic angle and negatively with TTJ tetanic extension (**Table 4)**. Higher pelvic angles imply reduced range of motion associated with imbalanced strength due to selective flexor hypertrophy and extensor weakness. Using TTJ extension as a surrogate for effects in extensor muscles as a whole, the opposite negative correlation with TTJ extension would be expected.

In considering the VL of grouped GRMD and normal dogs, we again expected to see a differential effect between TTJ extensor and flexor tetanic force. Instead, p62 levels correlated negatively with both values (**Table 4**). Decreased autophagic activity implied by higher p62 values could more broadly impair the regenerative response of dystrophic muscle over and above its effect on muscle degradation. Expression levels of p62 also correlated negatively with pelvic angle but positively with TTJ angle, in keeping with reduced range of motion in the pelvis and an opposite effect on the TTJ angle. The association between p62 expression and these angles likely reflects relative inefficiency in clearing cellular debris and damaged organelles during muscle repair.

Depending on the muscle involved and timing of disease, impaired autophagic activity could have either deleterious or beneficial effects.

Table 4. Autophagy protein expression at 6 months of age correlates with phenotype.

Genotype	Muscle	Variable	by Variable	Spearman ρ	Prob>|ρ|
Normal & GRMD	CS	TTJ Tetanic Flexion (N/KG)	LC3B-II	-0.827	0.002
Normal & GRMD	CS	CS Circumference (MM/KG)	LC3B-II	0.772	0.005
Normal & GRMD	CS	Eccentric Contraction Decrement (%)	LC3B-II	0.618	0.043
Normal & GRMD	CS	TTJ Tetanic Extension (N/KG)	p62	-0.954	<0.001
Normal & GRMD	CS	CS Circumference (MM/KG)	p62	0.890	<0.001
Normal & GRMD	CS	Pelvic Angle (º)	p62	0.814	0.004
Normal & GRMD	CS	TTJ Angle (º)	p62	-0.762	0.006
Normal & GRMD	CS	TTJ Tetanic Flexion (N/KG)	p62	-0.736	0.010
Normal & GRMD	CS	Eccentric Contraction Decrement (%)	p62	0.727	0.011
GRMD	CS	Pelvic Angle (º)	p62	0.985	<0.001
GRMD	CS	TTJ Tetanic Extension (N/KG)	p62	-0.942	0.005
Normal & GRMD	VL	TTJ Tetanic Flexion (N/KG)	p62	-0.727	0.011
Normal & GRMD	VL	Pelvic Angle (º)	p62	0.734	0.016
Normal & GRMD	VL	Eccentric Contraction Decrement (%)	p62	0.690	0.019
Normal & GRMD	VL	TTJ Tetanic Extension (N/KG)	p62	-0.681	0.021
Normal & GRMD	VL	TTJ Angle (º)	p62	-0.642	0.033

3.3.5 Spatial Expression of LC3B in Canine Skeletal Muscle

Our Western blot data indicate that muscles from 6-month-old GRMD dogs have increased LC3B-II and p62 protein levels. Measurement of static levels of these proteins in skeletal muscle does not allow definition of where the material is accumulating, nor whether there is truly increased autophagic activity or decreased autophagic flux and pathway dysregulation. So as to better make this distinction, we used light and TEM to localize LC3B-positive autophagic structures in the differentially affected cranial CS and VL muscles of 6-month-old GRMD dogs.

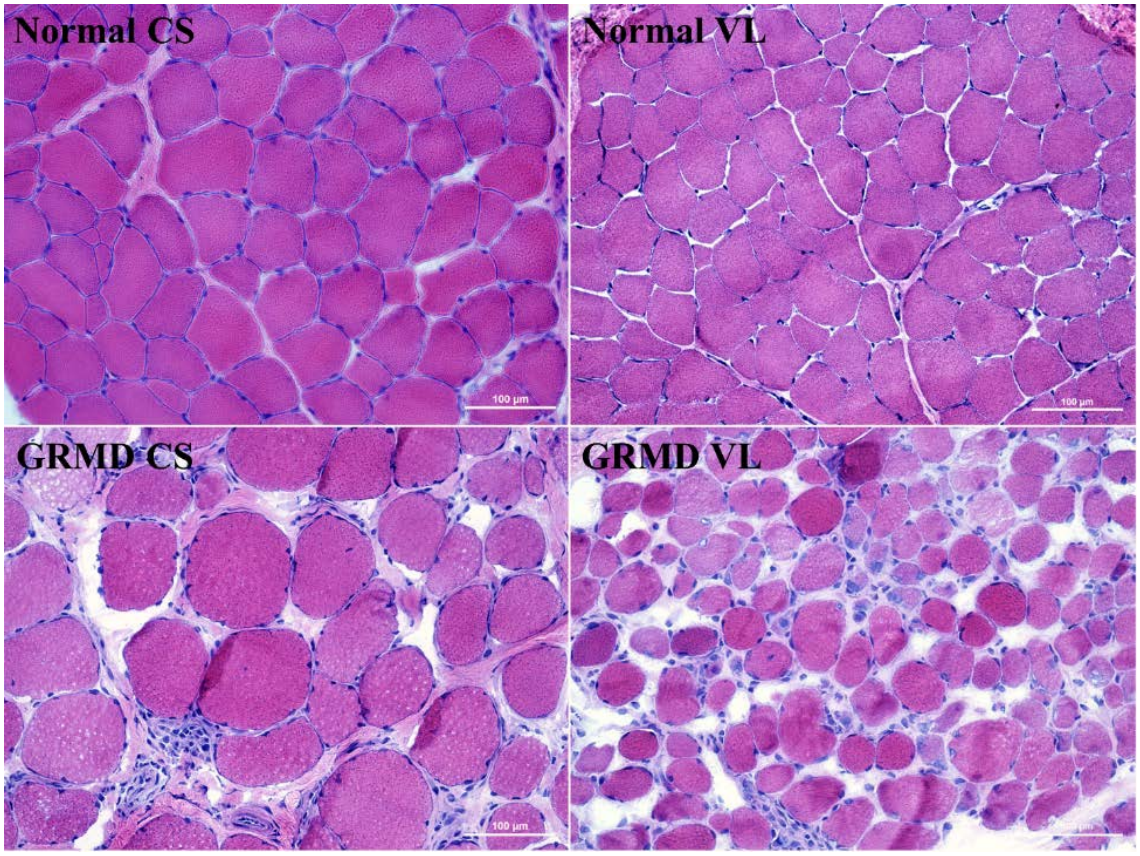

Figure 11. H&E muscle section of the CS and VL at age 6 months in normal and GRMD dogs. Note the phenotypic variation characterized by the hypertrophied muscle fibers in the GRMD CS and the atrophied fibers in the GRMD VL.

Classical small group muscle necrosis and regeneration typical of dystrophin–deficient muscle was seen on H&E sections **(Figure 11)**. Myofibers in the CS were hypertrophied, while those of the VL were atrophied. Occasional myofibers in each section of both muscles exhibited abundant punctate LC3B positive (~1 um) foci, consistent with autophagic vacuoles (**Figure 12**). These vacuoles were primarily seen in hypertrophied, hypercontracted (e.g., hyaline) fibers and degenerative muscle cells invaded with macrophages but also occurred in inflammatory cells within the interstitial space.

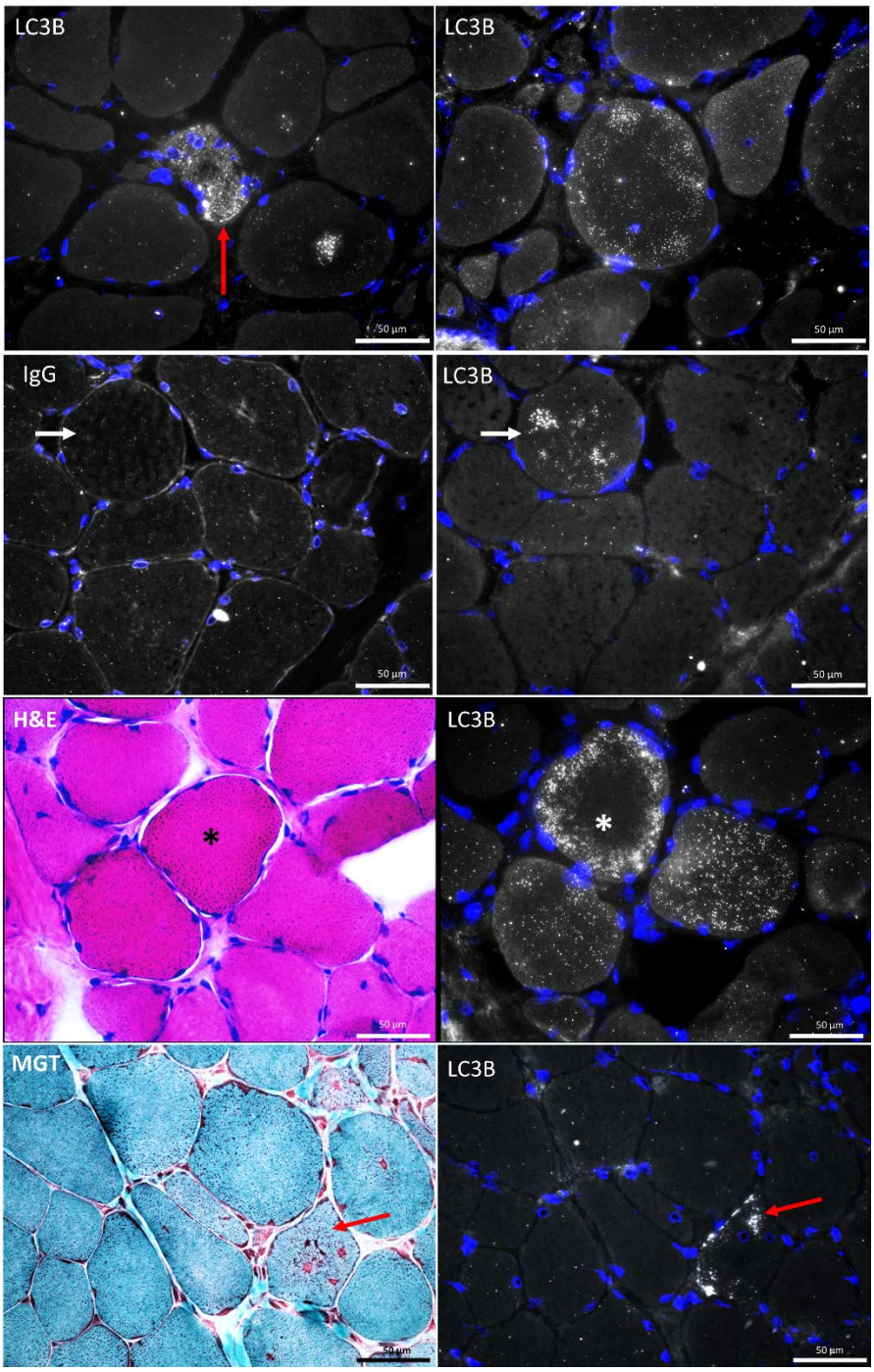

Figure 12. LC3B immunofluorescence in the 6-month-old GRMD CS. Top Panel: Light microscopy immunofluorescence for LC3B in the GRMD CS revealed punctate signals in degenerative muscle fibers and invading inflammatory cells (red arrow). Normal IgG served as the negative control and supported the LC3B antibody specificity (white arrows). Bottom Panel: Serial sectioning and staining with H&E and modified Gomori trichrome of the GRMD CS at age 6 months revealed that the LC3B positive cells were characteristically degenerative fibers (asterisks) with peripheral staining (red arrows).

Interestingly, LC3B positive foci were seen in occasional myofibers of normal VL muscle but not the normal CS (**Figure 13**), perhaps related to the fiber type (i.e., slow- vs. fast-twitch) makeup of the muscle [79]. The CS and VL are mixed muscles, so fiber type would not be expected to play a major role in the differential pattern of autophagic vacuole distribution. However, we typically sample the periphery of the VL muscle away from the bone, where there is a higher percent of fast-twitch fibers [49].

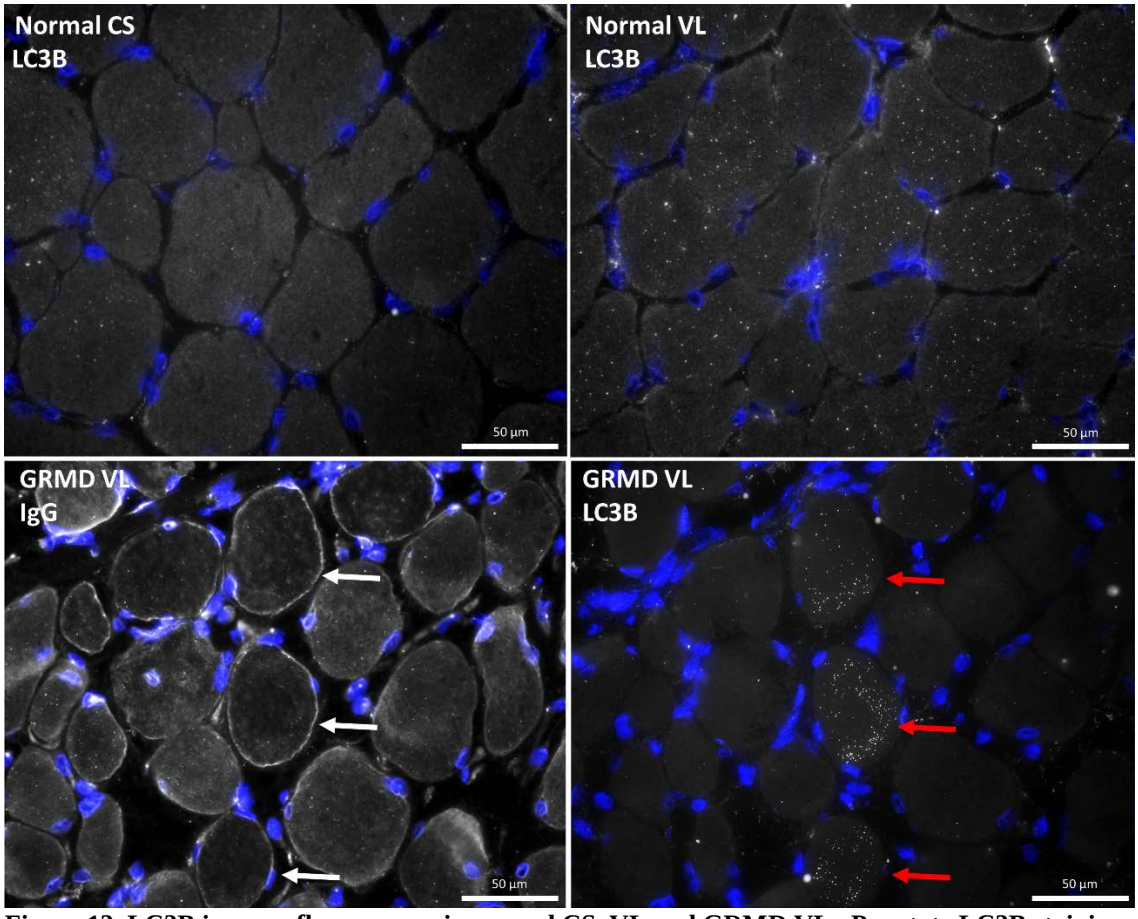

Figure 13. LC3B immunofluorescence in normal CS, VL and GRMD VL. Punctate LC3B staining is more prominent in the normal VL than the normal CS at age 6 months. LC3B staining is localized to rare, specific myofibers (red arrows) in the GRMD VL. Note the absence of punctate staining in the IgG negative control (white arrows).

We pursued the possibility that fiber type was playing a role by investigating the myosin heavy chain (MHC) fiber type of the LC3B-positive myofibers. LC3B-positive fibers present in the dystrophic CS (**Figure 14**) and VL (**Figure 15)** and normal VL muscles were consistently positive for fast-twitch MHC antibody, in keeping with prior studies showing that fast fibers have greater autophagic activity [79].

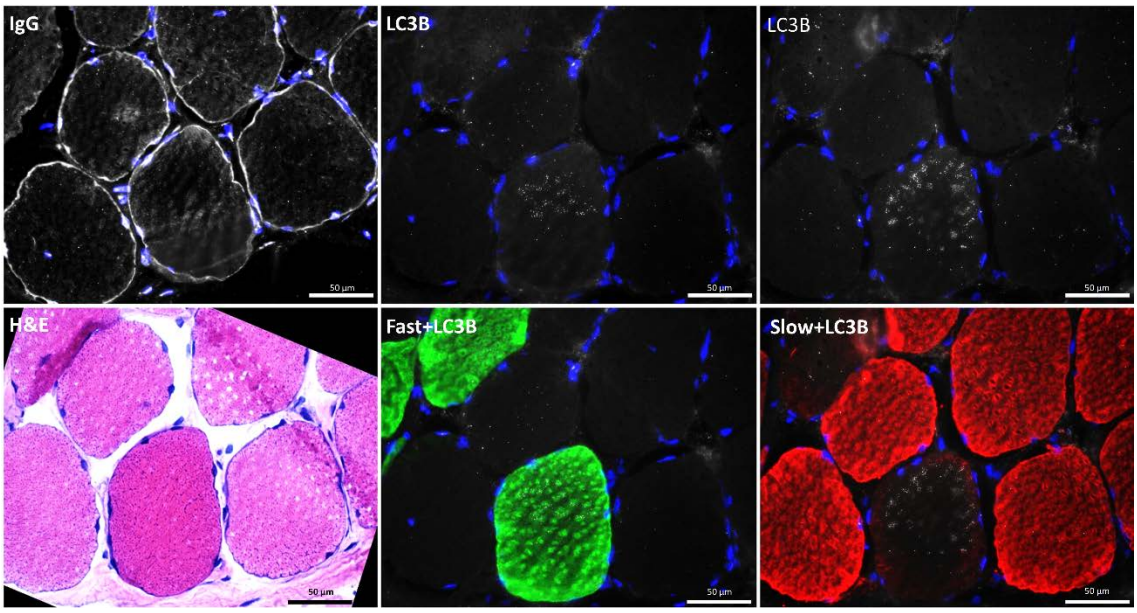

Figure 14. Immunofluorescence staining for LC3B and MHC fiber-typing in GRMD CS.MHC fiber-typing in the CS of 6-month-old GRMD dogs revealed proportionally more slow-twitch fibers compared to normal. Double immunostaining for LC3B and MHC fiber-typing revealed LC3B puncta were predominately in fast-twitch fibers.

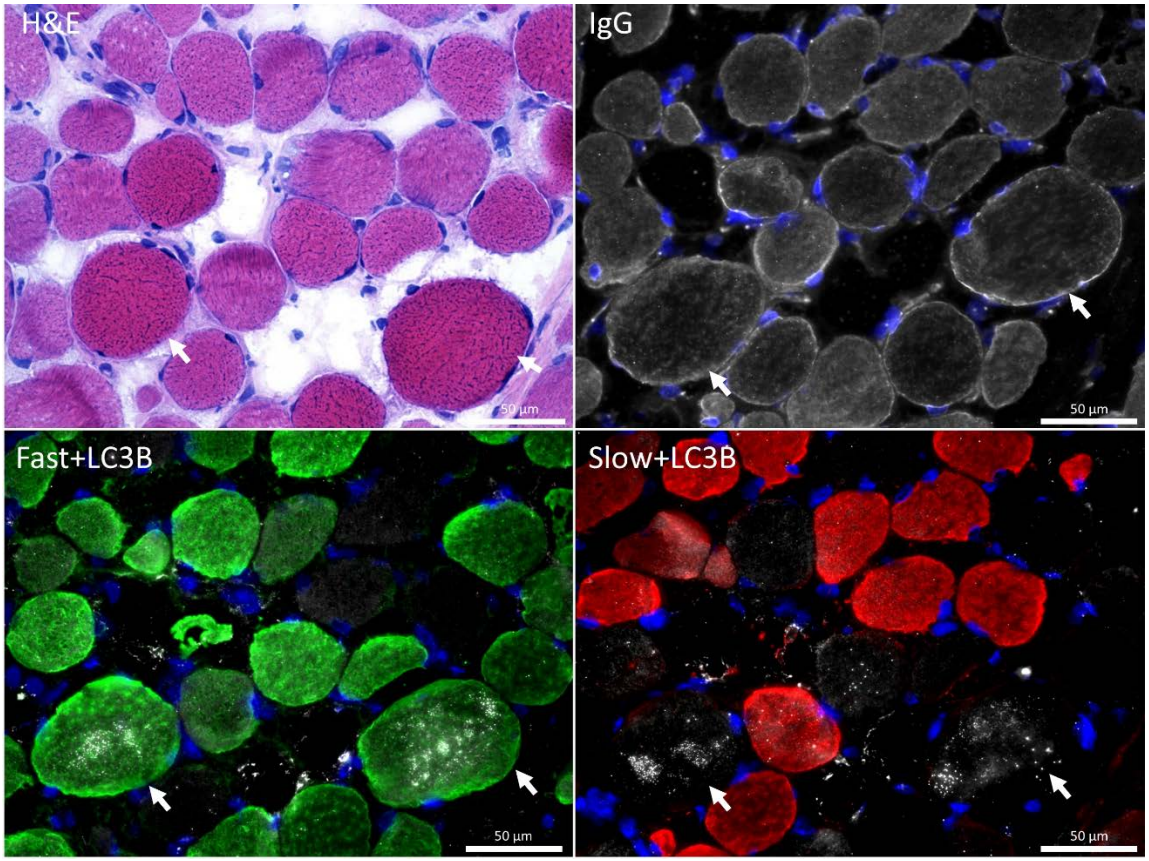

Figure 15. Immunofluorescence staining for LC3B and MHC fiber-typing in GRMD VL. LC3B staining in the GRMD VL at age 6 months is concentrated to degenerative fibers (white arrows) and cells in the interstitial spaces. The LC3B positive fibers are predominately fast-twitch based on MHC fiber typing and the IgG staining serves as the negative control.

The proportion of slow-twitch muscle fibers was increased in GRMD muscle, consistent with the slow-fiber predominance reported previously in DMD and GRMD. Many of the fibers stained for both slow- and fast-MHC markers, reflecting the muscle's attempt at regeneration and necessary fiber type switching (**Figure 16)** [80, 81].

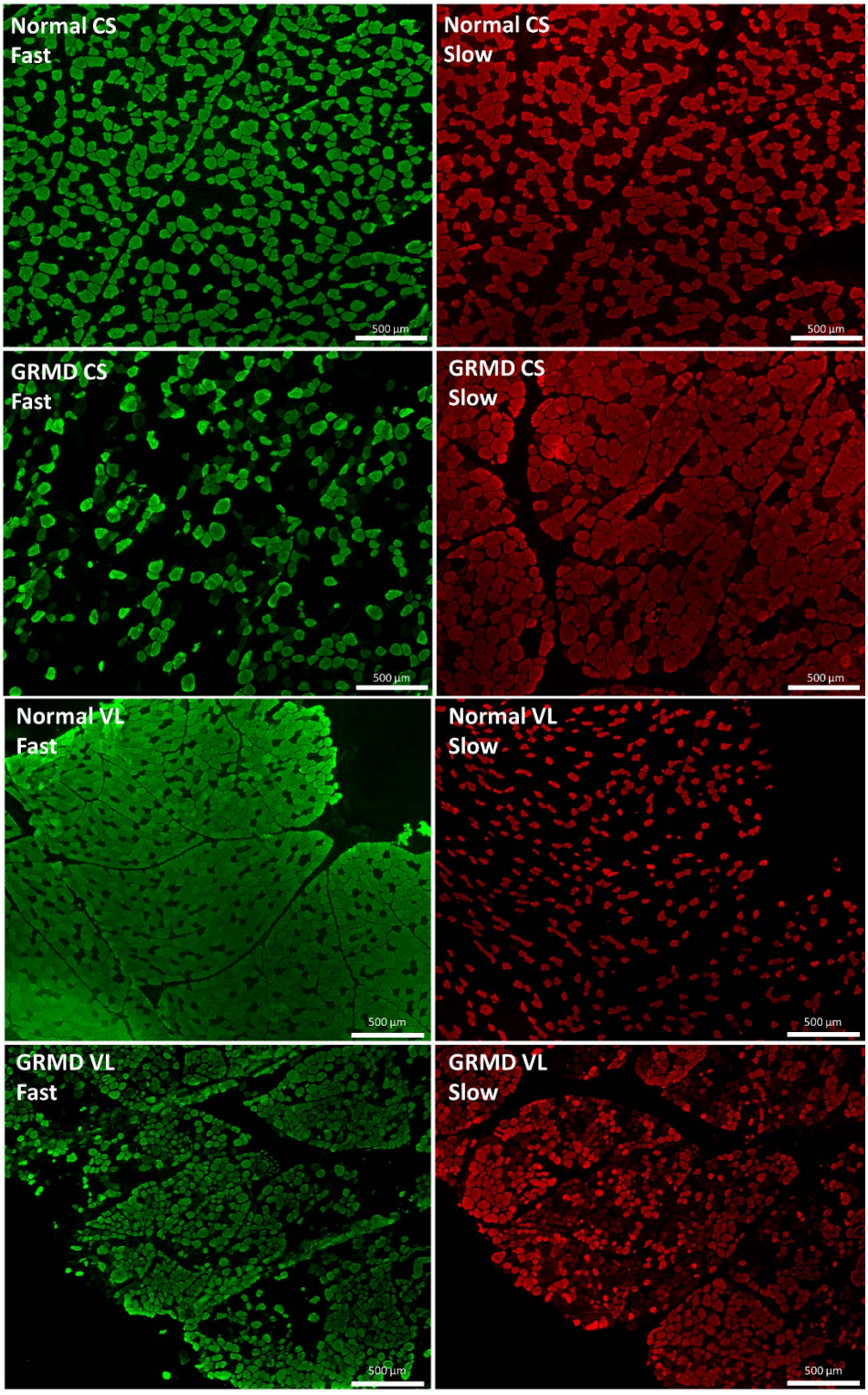

Figure 16. MHC fiber-typing in the CS and VL of normal and GRMD dogs. MHC fiber-typing in GRMD muscles at age 6 months revealed proportionally more slow-twitch fibers in the CS and fewer fast-twitch fibers in the VL, compared to normal.

3.3.6 Ultrastructural Analysis of GRMD Skeletal Muscle

To further characterize the nature and morphologic distribution of LC3B positive foci (i.e., autophagic vacuoles), we conducted ultrastructural studies, focusing on thick sections with hyaline fibers and fiber degeneration. Indeed, we identified classic double membrane-bound autophagosomes containing debris in degenerating fibers (**Figure 17A**) but rarely in normal appearing fibers. Furthermore, we identified autophagic vacuoles, residual bodies, and myelin figures in degenerating myofibers (**Figure 17B)**, a single neuromuscular junction (**Figure 17C)**, and local inflammatory cells (**Figure 17D, Figure 17E**). These structures were present in the cytoplasm near the sarcolemma of myofibers, consistent with the LC3B immunofluorescence staining pattern. Macrophages, both within the extracellular space (**Figure 17D)** and necrotic myofibers (**Figure 17E),** contained vacuolated structures typical of lysosomes, phagosomes and autophagic vacuoles, as previously reported (69). Taken together, the residual bodies, myelin figures, and autophagic vacuoles in degenerative fibers and inflammatory cells likely contributed to the LC3B signal identified by western blot and immunofluorescence[82]. These structures would be expected in degenerative muscle and could be consistent with impaired autophagy, although they do not, in themselves, reflect a disordered or inappropriate autophagic response.

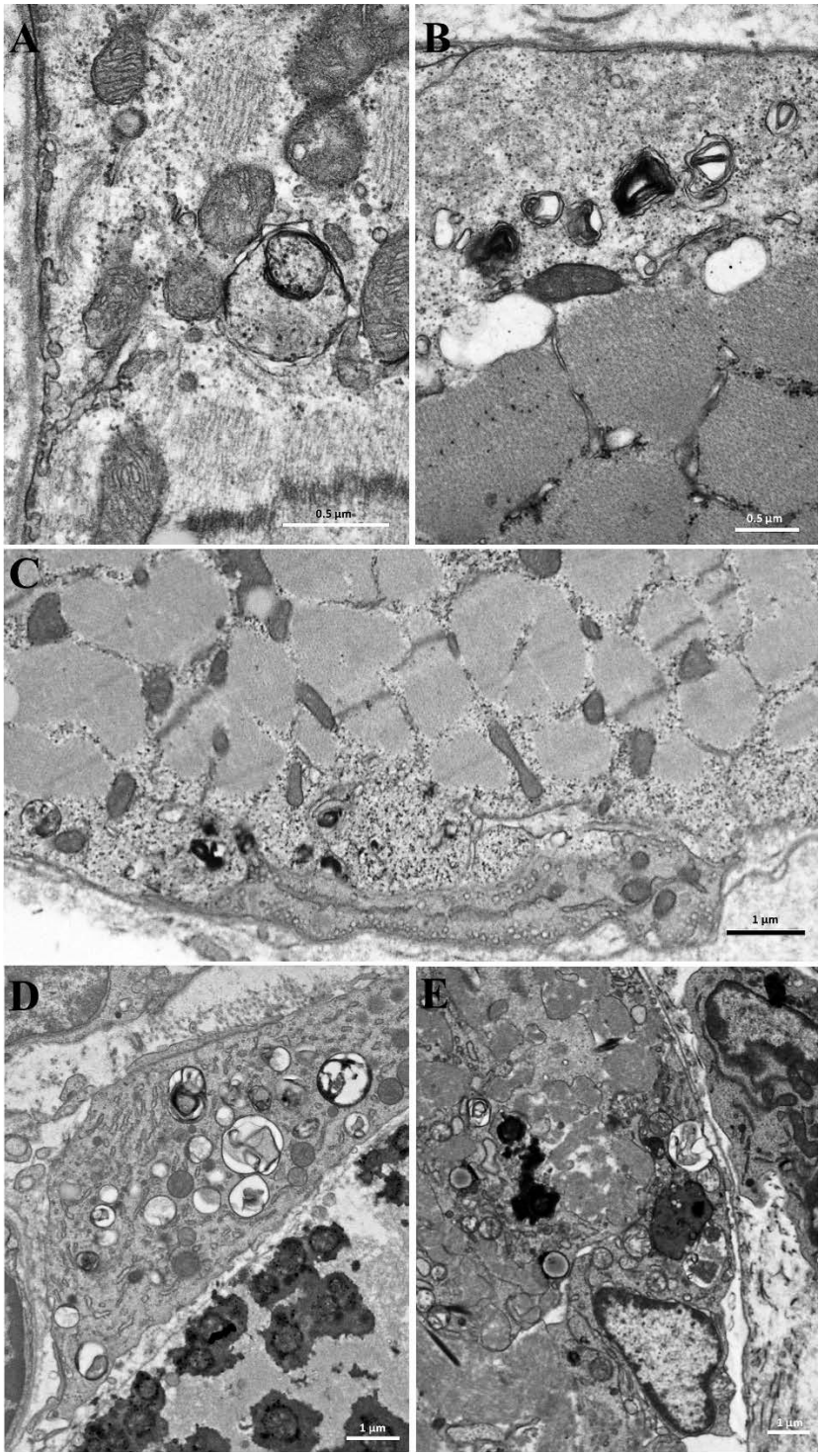

Figure 17. TEM images of 6-month-old GRMD CS and VL. A) Autophagic vacuole containing cargo identified in a GRMD VL myofiber. B) Myelin figures and residual bodies in a GRMD CS myofiber. C) GRMD CS neuromuscular junction containing residual bodies. D) Phagosomes in a macrophage located outside a necrotic myofiber. E) Autophagic vacuoles and phagosomes in a necrotic myofiber invaded with inflammatory cells.

In summary, the minimal evidence of LC3B-positive structures with immunofluorescence and absence of autophagosomes on ultrastructural assessment matched our gene expression results suggesting down-regulation of autophagy. Similarly, the increase in both LC3B-II and p62 protein was in keeping with either compromised autophagic activity or an overwhelmed autophagic system.

3.4 Discussion

Disordered autophagy has been incriminated in the pathogenesis of a number of diseases [23]. Studies in the dystrophinopathies have mostly focused on the mdx mouse, in which autophagy is generally felt to be down-regulated but varies somewhat among muscles. For example, autophagy was normal in the diaphragm but impaired in the tibialis anterior [61]. Overall, inadequate removal of damaged proteins and organelles is thought to contribute to a more severe mdx phenotype. Supporting this notion, therapies directed at enhancing autophagy have been beneficial [58-64].

Importantly, there is a fine line between true cell death by autophagy and the failed attempts of autophagy to ‘save’ the cell, ultimately leading to necrosis or apoptosis [83]. More than likely, dysregulated autophagy contributes to the cell’s ultimate fate by failing to clean up the accumulating damaged organelles and proteins. Another unique mechanism of autophagic cell death, involving extracellular ATP (i.e., damage-associated molecular pattern), heat-shock protein and the purinergic receptor P2X ligand-gated ion channel 7 (P2RX7), has been proposed in the mdx mouse [64]. In this context, the dystrophic muscle could take a ‘double hit’ potentially beginning with

inherent dysregulated autophagy and compounded by membrane fragility caused by the absence of dystrophin.

In contrast to the mdx mouse, autophagy and UPS gene expression were comparable in most GRMD and normal muscles. However, as with a number of our other studies [11, 43], the GRMD CS muscle had a distinctive pattern. Levels of the FOXO3 regulated genes, *MAP1LC3B, ATG12,* and *BNIP3*, were lower than normal, especially at 3 months of age, when the CS is still recovering from early necrosis [43]. Interestingly, at 6 months of age, when the CS has stabilized and uniquely hypertrophied, autophagy gene expression remained lower than normal. Importantly, levels at this age correlated negatively with the degree of hypertrophy, pointing to a potential causal association. This association between autophagy and CS hypertrophy could be tied to Akt/mTOR activation, which serves as the master regulator of autophagy and is involved in muscle regeneration and hypertrophy in the mdx mouse and GRMD dog [11, 84, 85].

Beyond our studies of autophagy gene expression, we studied LC3B-II and p62 protein expression to better characterize autophagic flux [24]. Based on the mdx literature and our GRMD gene expression findings, we hypothesized that autophagy is lower in GRMD muscle, as evidenced by decreased levels of LC3B-II and increased p62 [58]. Surprisingly, LC3B-II levels in the GRMD CS were increased over normal, suggesting increased flux, decreased clearance (e.g., lysosome dysfunction), or an overwhelmed autophagic system. Levels of the p62 protein, which is relatively specific for autophagic activity, were also higher in GRMD dogs, consistent with decreased

autophagic flux. To better understand the functional consequences of dysregulated autophagy, we correlated protein expression and phenotypic data. Most notably, p62 tracked positively with GRMD CS circumference, drawing an association between impaired autophagosome clearance and inappropriate muscle hypertrophy.

Importantly, gene and protein expression data do not allow definition of involved cells. While autophagy may be impaired in dystrophic muscle cells, it may also be activated in invading inflammatory cells, creating a mixed signal. Moreover, lipids, lipofuscin and residual bodies seen on ultrastructural analysis can give an LC3 signal [82]. We utilized light and ultrastructural microscopy to better understand the spatial component of autophagy in GRMD muscle. Consistent with other studies, autophagy varied between muscle types, being higher in fast-twitch fibers. In this context, the shift from fast- to slow-twitch muscle fibers in dystrophic muscle could contribute to apparent autophagy dysregulation. Beyond the fiber type specificity, LC3B positive puncta were seen in degenerating myofibers and inflammatory cells involved in the clean-up process. As discussed earlier, considering autophagy's role in cell survival, basal dysfunction could predispose myofibers to the "double hit" of membrane fragility caused by dystrophin's absence. Our ultrastructural findings were nonspecific and more consistent with necrosis (e.g., damaged sarcolemma, swollen mitochondria and sarcoplasmic reticulum); however, the presence of autophagic vacuoles, residual bodies, and myelin figures could be clues to support cell death by autophagy [64] or impaired autophagosome clearance (e.g., lysosome dysfunction) [62, 86]. This would be further

compounded by continuing cellular stress [87] and the role that autophagy plays with the monocyte-macrophage system in the cleanup process [88-90].

Our serial gene expression studies at different ages provided insight on changes associated with autophagy gene regulation as the disease progressed. Additionally, by correlating gene and protein expression levels with phenotypic findings, we were able to infer certain disease associations (e.g., CS hypertrophy). Importantly, these GRMD data are static measurements of autophagic activity. An autophagy flux assay, utilizing drugs like chloroquine, would be required to assess the movement of material through the autophagic pathway. Further limitations include our failure, thus far, to analyze autophagy related signaling proteins (e.g., Akt, p-Akt, mTOR, Beclin-1), small sample sizes inherent to large animal studies, and the lack of normal canine muscle for transmission electron microscopy.

In conclusion, our data suggest that autophagy is impaired in at least certain muscles of GRMD dogs. Basal autophagy dysregulation could place the fragile dystrophic myofiber at added risk, which would be further compounded by defective cleanup of cell debris. The differential involvement of the GRMD CS emphasizes that therapeutic modulation of autophagy must be carefully considered and could require specific targeting. Our microscopic findings point to the shortcomings of interpreting gene and protein expression data alone, which do not allow definition of cells of origin. LC3B positive puncta seemed to cluster together, and where typically identified in degenerating myofibers and invading inflammatory cells, resulting in a mixed signal. These findings highlight the importance of utilizing a multi-modal approach to verify the

cellular sources of autophagic activity in skeletal muscle. Further investigation is required to determine if autophagy induction would be beneficial in GRMD.

Our findings in GRMD support previous reports that indicate loss of dystrophin results in a dysfunctional lysosome system [62, 86]. Without functional lysosomes, autophagy cannot effectively ‘clean-up’ and recycle damaged organelles and proteins, resulting in ultimate failure of autophagy activation. Therefore, future investigations should include evaluation of lysosome biogenesis regulation (e.g., transcription factor EB [*TFEB*]) and protein expression (e.g., lysosomal-associated membrane protein-1 [LAMP-1]) in GRMD skeletal muscle.

4. NBD PEPTIDE THERAPY MODIFIES AUTOPHAGY IN GOLDEN RETRIEVER MUSCULAR DYSTROPHY

4.1 Introduction

Duchenne muscular dystrophy (DMD) is an X-linked genetic disorder caused by mutations in the *DMD* gene that results in the absence of the dystrophin protein [91-93]. Dystrophin is essential for linking the muscle cytoskeleton to the extracellular matrix [2]. Without dystrophin, skeletal muscle undergoes progressive cycles of degeneration and regeneration, with consequent weakness, debilitating contractures and terminal respiratory and/or cardiovascular failure. Currently, treatments are palliative, consisting of corticosteroids and physical therapy [3]. Corticosteroids cause deleterious side-effects, prompting development of alternative pharmacologic strategies. Animal models, particularly the mdx mouse and golden retriever muscular dystrophy (GRMD) dog, play a key role in testing these treatments [94].

Corticosteroids act, in part, by blocking NF-κB signaling, which otherwise contributes to inflammation in dystrophin-deficient muscle [95]. A number of other treatments have been employed to inhibit NF-κB signaling [96]. One particular compound, the Nemo binding domain (NBD) peptide, blocks NF-κB by inhibiting assembly of the inhibitor of kappa B kinase (IKK) complex (i.e., IKKα and IKKβ) [97]. Mdx mice treated with NBD peptide improved muscle function and pathology [98-100]. A follow up study of GRMD dogs also showed NBD benefit [101].

Recently, macroautophagy (hereafter known as autophagy) has been investigated as a novel therapeutic target in DMD [27, 58, 61, 64, 102, 103]. Similar to NF-κB signaling, autophagy is a conserved biological mechanism essential for eukaryotic cell survival and homeostasis. Post-mitotic cells (e.g., myofibers and neurons) are more susceptible to disruptions in autophagy. Furthermore, data from mdx mice have shown that altered autophagic flux contributes to disease pathogenesis [58-64]. Autophagy and NF-κB pathways regulate each other in a context-dependent manner, with the potential for both inhibition and induction [104-108]. However, little is known about the crosstalk between these 2 processes in dystrophic muscle.

We sought to address this void by studying autophagy gene and protein expression in skeletal muscle of GRMD dogs previously treated with NBD [101]. While autophagy gene expression was increased in a muscle-dependent way in treated versus untreated GRMD dogs, protein levels did not differ consistently. Autophagy modulation with NBD treatment correlated with improved GRMD phenotype, but this effect also varied among muscles. Further investigation is required to determine the role NF- κB inhibition in modulating autophagy in skeletal muscle.

4.2 Materials and Methods

4.2.1 Animals

Dogs were cared for and assessed according to principles outlined in the National Research Council Guide for the Care and Use of Laboratory Animals. Dogs used in these studies were from a colony at the University of North Carolina at Chapel Hill

(UNC-CH) that was subsequently moved to Texas A&M University (TAMU). NBD studies performed at UNC-CH were approved by the UNC-CH Institutional Animal Care and Use Committee (IACUC) through protocol: NF-kB Inhibition Therapy for Duchenne Muscular Dystrophy (10-060). Control data were from natural history studies approved through IACUC protocol entitled, "Natural History and Immunological Parameters in the German Shorthaired Pointer Muscular Dystrophy (GSHPMD)" (09-011). Overall animal care and biomarkers used to characterize phenotype were covered by IACUC protocol entitled, "Standard Operating Procedures—Canine X-Linked Muscular Dystrophy" (09-351). The GRMD genotype was originally suspected in newborn pups based on elevation of serum creatine kinase (CK) and confirmed by polymerase chain reaction (PCR), as previously described [5].

The experimental design and results of the GRMD study have been described [101]. Briefly, dogs were treated intravenously 3 times weekly from ages 2 to 6 months [101]. Functional data and histopathologic lesion scores from the cranial sartorius (CS), vastus lateralis (VL), and diaphragm muscles were compared in 6-month-old NBD-treated and natural history controls (**Table 5**). These muscles were chosen because of their differential involvement in GRMD [43]. Muscle samples removed at biopsy or necropsy were snap frozen in isopentane, cooled by liquid nitrogen, and stored at -80ºC for future analysis. A total of 8 objective phenotypic biomarkers were collected at the time of biopsy or necropsy and included: pelvic angle; tibiotarsal joint (TTJ) angle; maximum hip flexion angle; maximum hip extension angle; TTJ tetanic flexion force;

TTJ tetanic extension force; percent eccentric contraction decrement; and, CS circumference [41].

4.2.2 RNA Extraction and Gene Expression

Total cellular ribonucleic acid (RNA) was isolated from frozen skeletal muscle samples utilizing TriPure Isolation Reagent (Roche, #11667157001) and tissue homogenization. RNA samples were DNase treated with Ambion Deoxyribonucleic Acid (DNA)-*free* kit™ (Applied Biosystems, #AM Total cellular ribonucleic acid (RNA 1906). RNA concentrations of the individual samples were measured using a Nanodrop 2000 spectrophotometer. RNA quality was assessed using a 2100 BioAnalyzer (Agilent Technologies) and all samples had a RIN > 9. Samples of skeletal muscle RNA (100 ng) were reverse transcribed into cDNA using oligo-dT, random octamer primers and the SuperScript® II Reverse Transcription Kit (Invitrogen, #18064-014). Primers were designed using the NCBI Primer-Blast tool to target spanning exons for 4 autophagy genes (*MAP1LC3B*, *ATG12*, *BCN1*, and *BNIP3*), 2 ubiquitin proteasome system (UPS) genes (*FBXO32*, *TRIM63*), and 1 housekeeping gene (*HPRT1*) (**Table 6)**. PCR primer efficiency was estimated using the LinRegPCR program (Version 2015.3) to ensure the primer pair amplification factor was >1.9 [69-71]. The qPCR was performed in triplicate reactions with Power SYBR® Green PCR Master Mix (Applied Biosystems, #4367659) on an Applied Biosystems 7900HY Fast Real-Time PCR System. Relative fold changes in gene expression between normal and GRMD muscles were calculated using the comparative C(T) method and the equation $2^{-\Delta Ct}$ with *HPRT1* as the house-keeping gene [72].

Table 5. Sample sizes for gene expression.

Muscle	Normal (n=)	GRMD (n=)	GRMD+NBD (n=)
CS	6	10	6
VL	4	10	6
Diaphragm	3	4	6

Table 6. Primers for qPCR.

Gene Name	Forward Primer	Reverse Primer
MAP1LC3B	TTCAAGCAGCGTCGCACCTT	GCTGTAAGCGCCTCCTAATGAT
ATG12	CCCGAACCATTCAAGGACTCA	CCCAGAGCTGTTTCCTTTGT
BCN1	TCAGGAGGAAGCTCAGTATCAGA	TGTGCCGAACTGTCCACTGT
BNIP3	AGCTCCCAGTCTGAGGAAGA	TTCCGGCCGACTTGACCAAT
FBXO32	TGACGTTGCAGCCAAGAAGA	CAGTTCCAACAGCCGCACAA
TRIM63	TGCTCCATGTGCAAGGTGTT	TGACTGTTCTCCTTGGTCACT
HPRT1	AGCTTGCTGGTGAAAAGGAC	TTATAGTCAAGGGCATATCC

4.2.3 Western Blotting

Protein expression of the autophagosome marker LC3B-II and the autophagy readout protein p62/SQSTM1 were evaluated in the same skeletal muscles, if available, using Western blotting [24]. Because of the number of samples, separate gels were run for the CS and VL (n=7 GRMD and 6 GRMD+NBD). All diaphragm samples (n=3 normal, 4 GRMD and 6 GRMD+NBD) were run in a single gel.

To prepare protein lysates, frozen muscle samples were homogenized in RIPA lysis buffer (Santa Cruz Biotechnologies, #sc-24948A) and stabilized with HALT™ protease and phosphatase inhibitor (Thermo Scientific, #78442). Samples were incubated on ice for approximately 45 minutes and then centrifuged at 10,000 g (4°C) for 10 minutes. Pellets were discarded and supernatants for each sample were designated as the crude total protein lysates. Protein lysate concentrations were estimated using the modified-Lowry method provided by the DC™ Protein Assay Kit (Bio-Rad, #5000112)

[45]. Protein lysates were mixed with reducing SDS sample buffer, heated at 96°C for 5 minutes, than ~60 µg/sample were loaded into 12% TGX Stain-Free™ polyacrylamide gels (Bio-Rad, #161-0185) for electrophoresis. The samples were run at 200 V for 45 minutes in the Mini-Protean® Tetra Cell (Bio-Rad, #165-8000) to allow for adequate separation of the protein profiles. To activate the TGX Stain-free gels prior to transfer, they were imaged on the Gel Doc™ EZ System (Bio-Rad, #1708270). Protein transfer was performed using the Mini Trans-Blot® system (Bio-Rad, #170-3930). A cooled, wet transfer at 100 V for 1 hour with Tris/Glycine/0.05% SDS and 20% methanol was performed. Quality transfer of the proteins to a methanol activated, 0.2-µm (pore size) PVDF membrane was verified using the Gel Doc™ EZ System (Bio-Rad, #1708270). After excellent protein transfer was verified, the PVDF membrane was cut into 2 pieces (>20 kDa and <20 kDa), which allowed for simultaneous probing for 2 autophagy-related proteins (LC3B and p62) of different molecular weights. The membrane was washed with Tris-buffered saline with tween (0.1% Tween 20)(TBST) for 10 minutes, then blocked with TBST containing 5% milk and 1% BSA for 1 hour at 20°C. Next, specific PVDF membrane pieces were washed for 10 minutes and then incubated for 1 hour at 20°C and ~17 hours at 4°C in blocking buffer containing LC3B antibody (Novus Biologicals, #NB100-2220) or p62/SQSTM1 antibody (Novus Biologicals, #NBP1-49954) with rocking. The membranes were then washed in triplicate with TBST, 10 minutes each. Membranes were subsequently probed with goat anti-rabbit HRP secondary antibody (Pierce, #31466) diluted at 1:10,000 in blocking buffer for 1 hour at 20°C. This was followed by triplicate 10-minute washes with TBST. Finally, the

membranes were incubated with enhanced chemiluminescence substrate SuperSignal® West Dura (Thermo Scientific, #37071) for 5 minutes at 20°C and imaged on the Gel Doc™ XR+ System (Bio-Rad, #1708195). A cumulative chemiluminescent protocol was used to collect 60 consecutive images starting at 10 seconds and ending at 600 seconds. The images were analyzed using the Image Lab™ software (Bio-Rad, Version 5.2). Normalization of band density for the protein of interest was performed by correcting for the amount of total protein loaded. This was estimated by measuring the total regional lane density identified on the PVDF membranes. Relative fold change in protein expression was normalized for protein loading by calculating the ratio of individual band density (e.g., LC3B-II, p62) and total lane density (LD).

4.2.4 Statistical Analysis

All values are expressed as means ± 95 % confidence interval. Statistical differences in gene and protein expression between muscles of normal, GRMD and NBD treated GRMD dogs were analyzed using a 1-way ANOVA. If a significant difference ($p \leq 0.050$) in means was identified among all 3 groups, paired comparisons were made with Student's t test ($p \leq 0.050$; no post hoc adjustments of p values were performed). Phenotypic correlations with gene and protein expression were analyzed with the Spearman's correlation test ($p \leq 0.050$). All analyses and graphs were created with JMP® Pro 11.1.1.

4.3 Results

4.3.1 Gene Expression in Muscles of GRMD Dogs Treated with NBD

Expression levels of the different autophagy genes differed from one another and among muscles in the treated and control dogs.

MAP1LC3B levels were significantly different among normal, GRMD and NBD treated GRMD dogs ($p = 0.002$). Based on comparisons between groups, *MAP1LC3B* was lower in the GRMD CS relative to normal ($p < 0.001$) and higher after NBD treatment ($p = 0.018$) (**Figure 18A**). A similar pattern in the VL and diaphragm did not reach significance.

BNIP3 levels in both the CS ($p < 0.001$) and VL ($p = 0.002$) were significantly different among normal, GRMD, and NBD-treated GRMD dogs. *BNIP3* levels in the CS were lower in GRMD ($p = 0.070$) relative to normal and higher after NBD treatment compared to both normal ($p < 0.001$) and GRMD dogs ($p < 0.001$) (**Figure 18B)**. *BNIP3* levels in GRMD VL were not different relative to normal ($p = 0.360$) but were higher after NBD treatment compared to normal ($p = 0.020$) and GRMD dogs ($p < 0.001$). A similar trend in the NBD-treated GRMD diaphragm was not significant.

BCN1 levels were significantly different among all groups in the CS ($p < 0.001$) and trended in the VL ($p = 0.070$). *BCN1* levels in GRMD CS were not different relative to normal but were higher after NBD treatment compared to normal ($p < 0.001$) and GRMD dogs ($p < 0.001$)(**Figure 18C).** Levels did not differ in the diaphragm.

ATG12 gene levels were significantly different among all groups in the VL ($p = 0.041$) but not in the CS ($p = 0.052$). *ATG12* levels in the VL were not different to normal but

were higher after NBD treatment compared to normal dogs (p = 0.013). Levels in the diaphragm did not differ among groups.

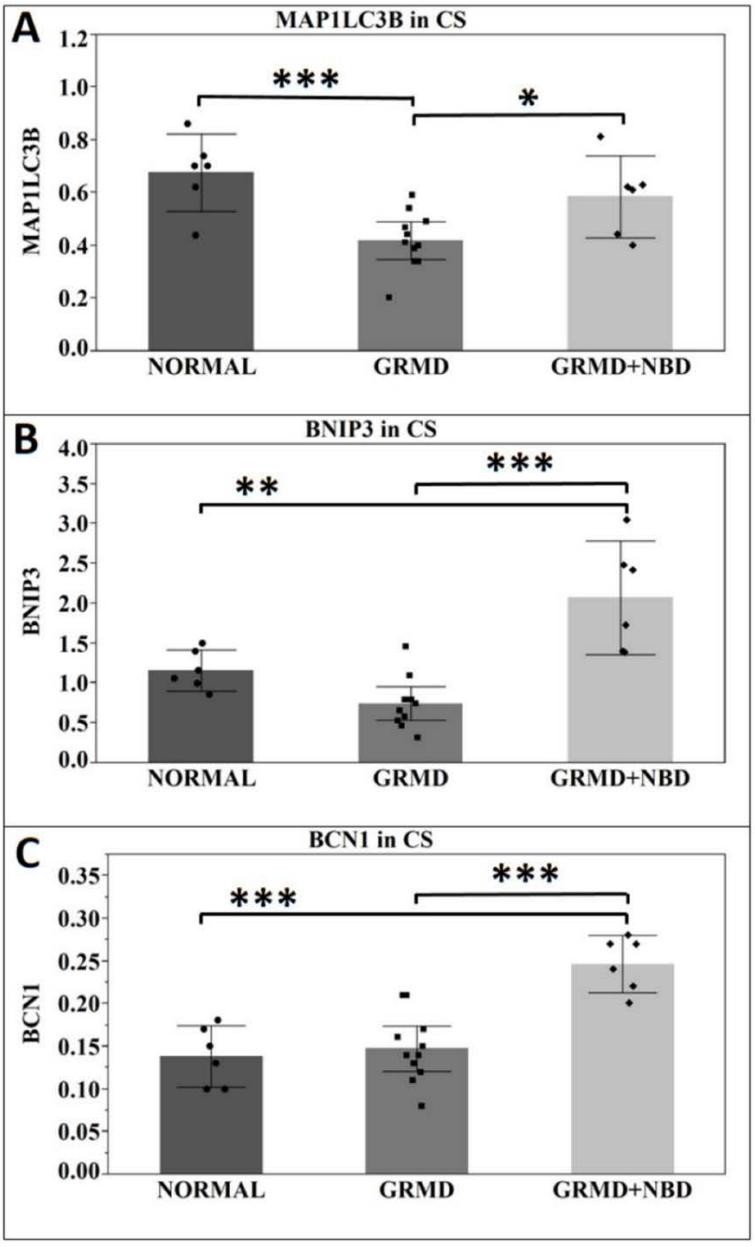

Figure 18. Autophagy gene expression in the CS of normal, GRMD, and NBD-treated GRMD dogs. A) MAP1LC3B gene expression was lower in GRMD and higher with NBD treatment. B) BNIP3 expression was higher in the GRMD CS with NBD treatment. C) BCN1 expression was higher in the GRMD CS with NBD treatment. Bar graphs represent mean expression +/- 95 % confidence interval. *p<0.050, **p<0.010, ***p<0.001.

The differential response of autophagy genes among muscles of NBD-treated GRMD dogs highlights the complexity of skeletal muscle homeostatic systems. The CS had a distinctive pattern, with values being lower in GRMD versus normal dogs and increasing with NBD treatment. We have previously shown that the GRMD CS undergoes early necrosis and hypertrophies by age 6 months of age [43]. Higher autophagy gene expression in treated CS of GRMD dogs implies that NBD-induced autophagy could facilitate clearance of damaged cellular debris. Lower levels in some muscles might simply reflect more delayed injury and regeneration. With this said, autophagy genes did not consistently track with one another. As an example, *BNIP3* levels were increased while those for *BCN1* were decreased in the VL of NBD treated GRMD dogs. These conflicting signals suggest dysregulation of the autophagy system.

Expression levels of the UPS genes, *FBXO32* and *TRIM63*, did not differ between normal and GRMD dogs, indicating a lack of UPS activation in dystrophic muscle consistent with prior studies [109]. With NBD treatment, levels for both genes were lower in the GRMD CS and VL, but the difference did not reach significance, likely due to a single outlier dog. Levels did not differ in the diaphragm, further emphasizing variation among muscles.

Table 7. Autophagy and UPS gene expression correlates with NBD treatment in GRMD dogs.

Muscle	Variable	by Variable	Spearman ρ	Prob >|ρ|
CS	Pelvic Angle (º)	*TRIM63*	0.8654	< 0.001
CS	Hip Flexion Angle (º)	*BCN1*	-0.7826	< 0.001
CS	TTJ Tetanic Extension (N/KG)	*TRIM63*	-0.7929	< 0.001
CS	TTJ Tetanic Extension (N/KG)	*BNIP3*	0.7529	0.001
CS	TTJ Tetanic Extension (N/KG)	*ATG12*	0.7235	0.002
CS	Hip Flexion Angle (º)	*TRIM63*	0.7234	0.002
CS	Pelvic Angle (º)	*BNIP3*	-0.7002	0.003
CS	TTJ Angle (º)	*ATG12*	0.6534	0.006
CS	Hip Flexion Angle (º)	*FBXO32*	0.6858	0.007
CS	Pelvic Angle (º)	*BCN1*	-0.6233	0.010
CS	Pelvic Angle (º)	*FBXO32*	0.6307	0.016
CS	Pelvic Angle (º)	*MAP1LC3B*	-0.5746	0.020
CS	Pelvic Angle (º)	*ATG12*	-0.5672	0.022
CS	Hip Flexion Angle (º)	*BNIP3*	-0.5483	0.028
CS	Hip Flexion Angle (º)	*MAP1LC3B*	-0.5203	0.039
CS	TTJ Angle (º)	*TRIM63*	-0.5323	0.041
VL	Pelvic Angle (º)	*BNIP3*	-0.6984	0.004
VL	Pelvic Angle (º)	*MAP1LC3B*	-0.5996	0.018
VL	TTJ Tetanic Extension (N/KG)	*BNIP3*	0.5786	0.024
VL	Hip Flexion Angle (º)	*BNIP3*	-0.573	0.026
VL	TTJ Tetanic Flexion (N/KG)	*FBXO32*	0.5879	0.035

To better understand NBD's therapeutic effects, we correlated gene expression and phenotypic tests. Phenotypic markers generally showed improvement with higher expression of *MAP1LC3B, ATG12, BCN1,* and *BNIP3* and lower expression of *FBXO32* and *TRIM62* (**Table 7**). This inverse relationship in autophagy and UPS gene expression may result from crosstalk between these 2 catabolic systems necessary for maintaining homeostasis [110-112]. Although gene expression might not reflect ongoing autophagic flux and proteasome activity, these findings provide interesting insight into NF-κB's role

in regulating muscle homeostatic systems and generally support a beneficial role for autophagy activation and UPS inhibition.

4.3.2 Autophagy Protein Expression in GRMD Dogs Treated with NBD

Expression of the autophagy proteins LC3B-II and p62 was studied in the same cohort described above. Based on our gene expression assays, we hypothesized that autophagic activity would be increased in NBD treated dogs. However, when a single outlier with a 3-fold increase in LC3B-II was excluded, LC3B-II activity was actually lower in the CS of NBD treated GRMD dogs (Fold Change = -1.43, p = 0.023) (**Figure 19A)**. This could reflect either increased autophagosome clearance or reduced autophagosome formation.

To better distinguish the underlying mechanism, we studied the autophagy readout protein p62. There was a trend towards lower values in treated versus control GRMD dogs (Fold Change = -2.1, p = 0.110) (**Figure 19B**). Lower p62 could be associated with increased autophagic flux. When interpreted with the tendency towards lower LC3B-II activity, this suggests that NBD induced autophagic activity, in line with our gene expression results.

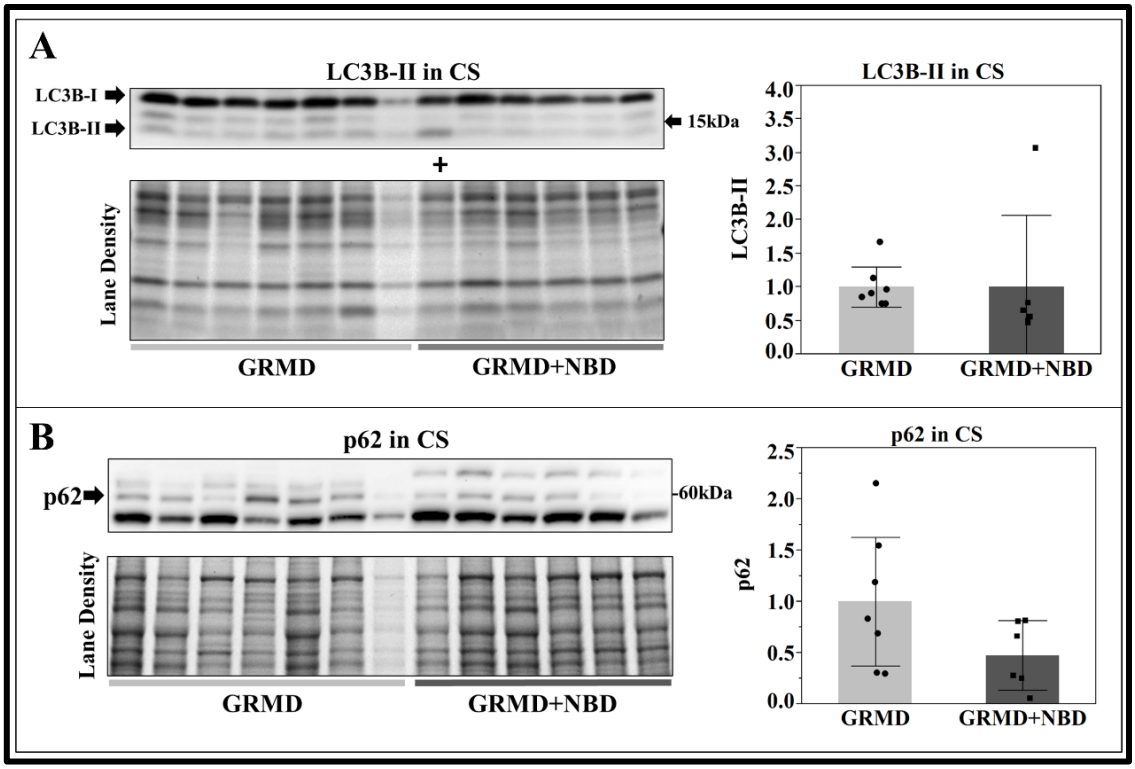

Figure 19. Western blots of LC3B and p62 in the CS of NBD-treated and control GRMD dogs. A) LC3B-II levels were lower with NBD treatment when a single outlier (+) was removed. B) p62 levels tended to be lower with NBD treatment. Bar graphs represent mean +/- 95% confidence interval.

In contrast, we found no significant difference in protein expression of LC3B-II (Fold Change = -1.43, p = 0.390; **Figure 20A)** and p62 (Fold Change = -1.25, p = 0.670; **Figure 20B)** in the VL of treated versus control GRMD dogs. As with the CS, expression levels varied remarkably among dogs. When the same outlier with increased LC3B-II VL expression was removed, LC3B-II levels were lower in NBD treated versus control GRMD dogs (Fold Change = -2.3, p = 0.049). Similarly, a single NBD-treated GRMD dog had a 2.8-fold higher p62 value relative to untreated GRMD dogs, while the other 5 dogs had relatively lower p62 expression. When this dog was excluded, the fold

change between the groups neared significance (Fold Change = -2.63, p = 0.058), in keeping with the pattern seen in the CS.

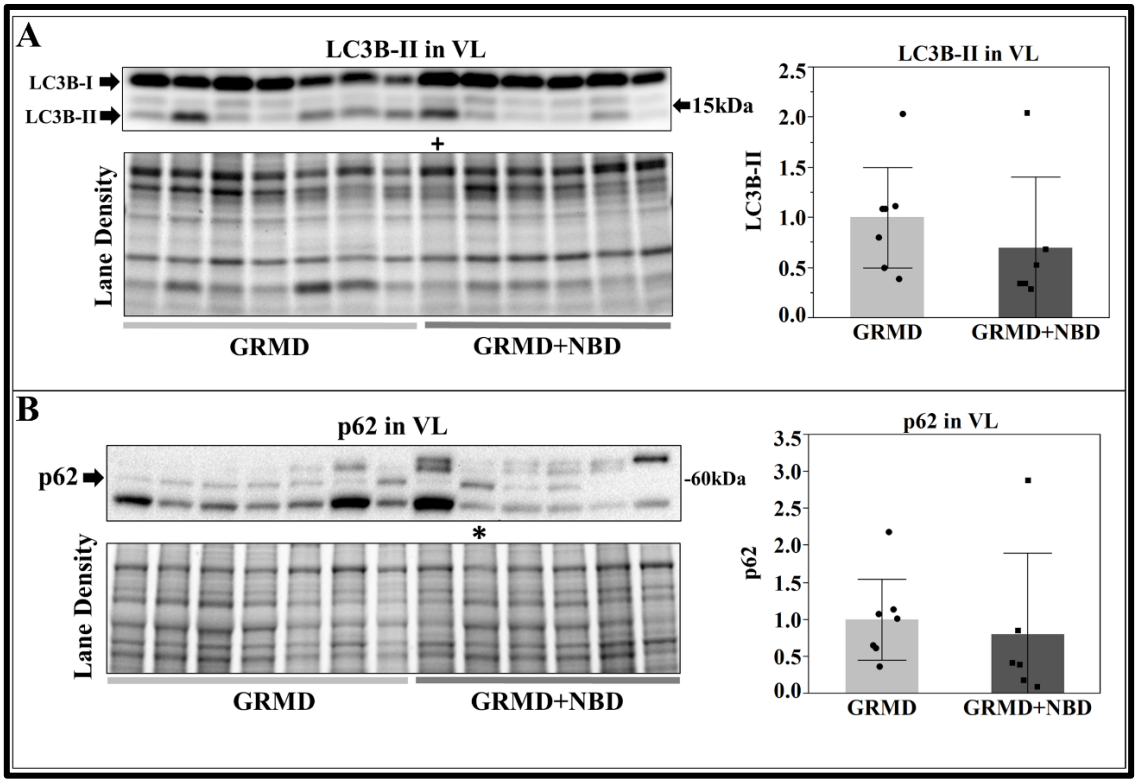

Figure 20. Western blots of LC3B and p62 in the VL of NBD-treated and control GRMD dogs. A-B) LC3B-II differed and p62 values approached significance when a single outlier (+ or *) was removed. Bar graphs represent the mean +/- 95% confidence interval.

Interestingly, we identified a significant ~32-fold difference in LC3B-II (p=0.006; **Figure 21A**) and a tendency towards higher (Fold Change = 10.0, p = 0.075; **Figure 21B**) p62 levels in the GRMD versus normal diaphragm. Concomitant increases in LC3B-II and p62 suggest that autophagic activity is impaired in the GRMD diaphragm at age 6 months. While values in NBD-treated and control GRMD dogs did not differ (p = 0.660; **Figure 21A**), there was a different pattern among treated dogs.

Two NBD-treated dogs had higher LC3B-II values, while the other 4 had lower levels relative to controls. On the other hand, p62 levels were increased (Fold Change = 3.3, p = 0.017; **Figure 21B**) in NBD-treated versus control GRMD dogs. Further increases of LC3B-II and p62 in NBD-treated GRMD diaphragm could exacerbate autophagic dysregulation, in contrast to apparent induction of autophagy in the CS and VL. This again points to differential effects of NBD treatment among GRMD muscles.

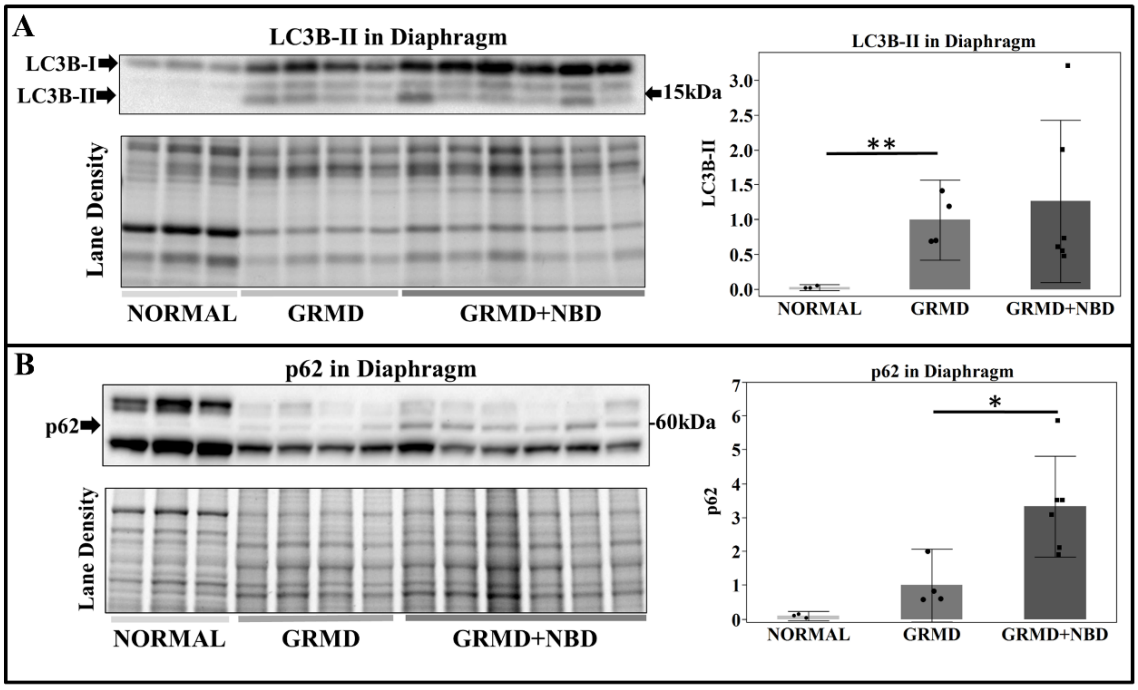

Figure 21. Western blots for LC3B and p62 in diaphragm of normal, GRMD, and NBD-treated dogs. A) LC3B-II is higher in GRMD versus normal dogs. B) p62 expression is higher in NBD treated versus control GRMD dogs. Bar graphs include mean +/- 95% confidence interval.

We next correlated phenotypic results with protein expression levels in the CS and VL of the combined control and NBD treated GRMD dogs. Although there were no significant correlations for LC3B-II expression, there was a tendency towards a positive

relationship (ρ = 0.552, p = 0.063) with CS circumference, in keeping with a role for autophagy in CS repair. Several significant correlations were identified for p62 expression in the CS and VL of GRMD dogs. Interestingly, CS p62 levels correlated positively with pelvic (ρ = 0.609, p = 0.035) and hip flexion (ρ = 0.607, p = 0.036) angles. Higher pelvic and hip flexion angles imply reduced range of motion. NBD treatment significantly decreased these angles [101]. Therefore, the apparent increase in autophagic activity associated with NBD treatment could be facilitating the repair response in the CS. Furthermore, VL p62 levels correlated negatively with TTJ tetanic extension (ρ = -0.601, p = 0.039). NBD treatment significantly increased TTJ tetanic extension levels in GRMD dogs [101]. Assuming that findings from the VL and TTJ extensors track together, increased autophagic activity implied by lower p62 values apparently aids in regeneration of dystrophic muscle. Furthermore, these changes complement the gene expression findings associating autophagy activation with NBD treatment in GRMD dogs. Further investigation is required to determine the exact role of NBD therapy in autophagy homeostasis.

In summary, NBD therapy in GRMD dogs increased autophagy gene expression in a muscle-dependent manner with additional changes in autophagy protein expression. Changes in the CS, in particular, correlated with certain phenotypic makers, consistent with a beneficial effect of autophagy. In contrast, effects in the diaphragm suggested that NBD could be further exacerbating autophagy dysregulation, highlighting variable treatment effects among muscles.

4.4 Discussion

In light of the absence of curative therapies for DMD, drugs aimed at ameliorating secondary effects (e.g., corticosteroids for inflammation) are often used. Drugs targeting autophagy could, in principle, promote clearance of cellular debris. Our findings suggest that NF-κB inhibition with the NBD peptide differentially modulates autophagy and UPS gene expression in GRMD skeletal muscle. The CS had a distinctive pattern, with values being lower in GRMD versus normal dogs and increasing with NBD treatment. We have previously shown that the GRMD CS undergoes early necrosis and hypertrophies by 6 months of age [43]. Higher CS gene expression implies that NBD-induced autophagy could facilitate clearance of damaged cellular debris. On the other hand, UPS gene levels tended to be lower in NBD-treated versus control GRMD dogs, consistent with reduced UPS activity and protein degradation. Such a reciprocal relationship is in keeping with the dual roles that autophagy and the UPS have in breaking down cellular components [113] and points to the complexity of these homeostatic systems in regulating Nf-κB activity.

Despite the changes in autophagy and UPS gene expression with NBD treatment, protein levels did not show consistent differences. This is not necessarily surprising, in that gene and protein expression do not necessarily track with one another [114]. Our ability to demonstrate differences was further complicated by wide variation in protein levels among NBD-treated dogs. Part of the variable response could be due to NBD peptide neutralization. As described in the original report, several GRMD dogs demonstrated hypersensitivity reactions to NBD [101], which could have blunted peptide

function. In line with this interpretation, careful analysis indicated that LC3B-II and p62 levels did decrease in some dogs, supporting increased autophagic activity. Furthermore, this decrease was primarily present in the NBD treated GRMD CS and VL, and was associated with clinical improvement. In contrast, NBD treatment led to significant increases in diaphragm p62, indicating that autophagy dysregulation may have been exacerbated.

Recent evidence indicates that distinct cell-type and context-specific roles for p62 can mediate NF-κB activity and inflammation [115]. Furthermore, an intrinsic regulatory loop that utilizes a NF-κB-p62-mitophagy pathway to restrain inflammation and favor repair has been described in macrophages [115]. Although NF-κB is classically considered the primary transcriptional activator of inflammatory genes, it also has anti-inflammatory properties [116, 117]. Therefore, in some cases, excessive inhibition of NF-κB could result in more inflammation and may explain the differential response between the CS, VL and diaphragm. Similarly, autophagic activity must be carefully regulated to maintain homeostasis, with for instance, either excessive or reduced autophagy ultimately resulting in muscle atrophy [102]. Therefore, treatments that modulate autophagy must be gauged to ensure that balance is restored.

Further studies are required to determine the interactions between autophagy regulation and NF-κB activation in dystrophic skeletal muscle. Utilizing normal and dystrophic canine skeletal muscle cell cultures to determine the effect of NF-κB modulation on basal and induced autophagy should be pursued.

5. CONCLUSION

5.1 Skeletal Muscle Homeostasis in GRMD

Duchenne muscular dystrophy (DMD) is an X-linked recessive genetic disorder caused by mutations in the *DMD* gene that results in absence of the dystrophin protein and cyclic muscle degeneration and regeneration. The 2 principal animal models used to explore novel therapeutics for DMD include mdx mice and golden retriever muscular dystrophy (GRMD) dogs [4]. Dogs with GRMD have a relatively severe phenotype that more closely mimics DMD compared to the mildly affected mdx mouse. Despite being caused by a single genetic mutation, GRMD displays dramatic phenotypic variation. For example, a litter of GRMD dogs can include both mildly and severely affected dogs that all have the same *DMD* gene mutation. This variability extends to the level of dystrophic muscles, with for instance, the cranial sartorius (CS) undergoing early necrosis and hypertrophy, while the vastus lateralis (VL) has a more delayed disease onset and atrophies [10, 11]. This phenotypic variation strongly suggests the influence of genetic modifiers that could serve as therapeutic targets.

Skeletal muscle homeostasis requires a delicate balance between protein synthesis and degradation (e.g., autophagy) and cell survival/programmed cell death (e.g., apoptosis). Autophagy and mitochondrial associated programmed cell death pathways, like apoptosis, have recently been identified as suitable secondary therapeutic targets for DMD. However, the role of these pathways in skeletal muscle homeostasis and variable disease progression in the dystrophinopathies remains to be elucidated. To

begin to address this gap in knowledge, we set out to learn more about the role of autophagy and apoptosis in GRMD pathogenesis.

5.2 Role of Apoptosis in GRMD Pathogenesis

First, we focused on the anti-apoptotic protein APIP, which was identified using a GWAS and our subsequent discovery of its role in other diseases [52, 56, 57]. APIP has at least 2 unique functions relating to its anti-apoptotic and enzymatic activities that could be relevant to muscle disease. APIP inhibits programmed cell death (i.e., apoptosis) through direct interaction with APAF-1, an activator of caspase-9 essential for apoptosome formation [35, 36]. In contrast to cell necrosis, apoptosis is tightly regulated process by which cells that are no longer needed can be destroyed without spilling their contents and inducing inflammation. In one sense, apoptosis is the more 'beneficial' way for cells to die. While necrosis is the terminal mechanism of cell death in DMD [37], the intrinsic apoptotic pathway is also activated in dystrophic myofibers in advance of necrosis [14].

Although we hypothesized that inhibition of apoptosis by APIP would be beneficial, VL levels tracked with a more severe phenotype (**Figure 22**). Furthermore, APIP was primarily expressed in slow-twitch muscle fibers of normal muscle and in regenerating fibers and inflammatory cells in dystrophic muscle. Expression in regenerating fibers could be tied to its anti-apoptotic activity or enzymatic role in methionine metabolism. The GRMD findings reported here support *APIP* as a candidate modifier gene, but we have not yet done further studies necessary to substantiate this

association. Sequencing of *APIP* might reveal novel structural characteristics that influence the biochemical functions of APIP, including its anti-apoptotic and enzymatic activity. Furthermore, evaluating the *in vitro* effects of APIP expression modulation on muscle cell growth and programmed cell death may help distinguish which function (i.e., anti-apoptotic &/or methionine salvage) of APIP is important in dystrophic muscle. These experiments are warranted to better define *APIP* as a candidate gene involved in the pathophysiology of dystrophic muscle and its novel role in muscle regeneration in response to damage.

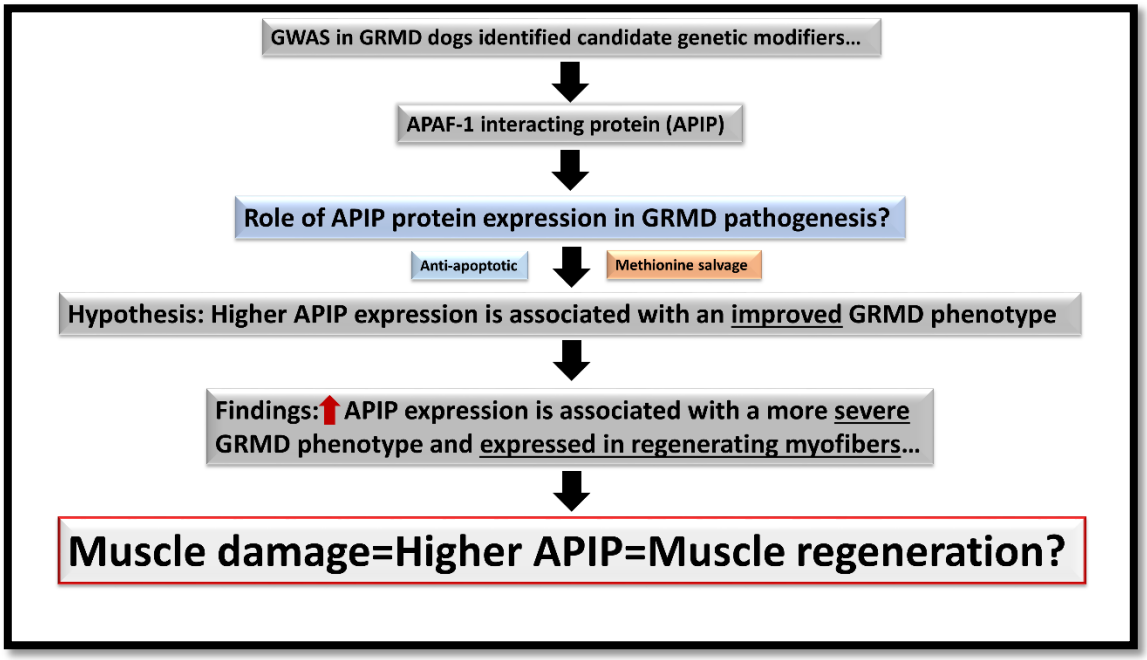

Figure 22. Schematic of the role APIP protein expression in GRMD pathogenesis.

5.3 Role of Autophagy in GRMD Pathogenesis

Next, we focused on the role of autophagy in GRMD pathogenesis. Autophagy is a conserved biological mechanism essential for survival of eukaryotic cells that involves organized degradation ("self-eating)" and recycling of cellular building blocks into macromolecules [21]. Tight regulation of autophagy is critical for maintaining homeostasis in skeletal muscle, with either too much or too little resulting in muscle atrophy and cell death [27, 28]. Based on the mdx literature, we hypothesized that autophagy would be lower in GRMD muscle, as evidenced by lower autophagy gene expression, lower levels of LC3B-II, and higher p62 levels [58]. Considering that the GRMD phenotype better mimics that of DMD, we sought to investigate autophagy in phenotypically distinct skeletal muscles from age-matched dystrophic and normal dogs. Of the autophagy genes studied, *MAP1LC3B* appeared to have the most consequential role in GRMD disease expression. Levels were lower in the GRMD CS at both 3 and 6 months of age correlated with CS circumference. This suggests that reduced CS autophagy could contribute to the classical true hypertrophy seen in this muscle.

To better establish overall autophagic activity, we also used Western blotting to assess the established autophagosome marker LC3B-II and the autophagy readout protein p62/SQSTM1. Contrary to our hypothesis, LC3B-II levels in the GRMD CS were higher than normal, indicating accumulation of autophagosomes from either increased flux, decreased clearance (e.g., lysosome dysfunction), or an overwhelmed autophagic system **(Figure 23**). We then assessed expression of p62, a readout protein relatively specific for autophagic activity. If autophagic flux were increased in the

dystrophic CS, p62 levels should be lower. Levels of p62 were significantly higher in GRMD dogs, consistent with decreased autophagic flux and correlated with a more severe phenotype. With normal balanced autophagy, increased LCB-II activity should track with decreased p62 expression. Taken together, our data suggest that autophagy is uniquely impaired in the CS and potentially other muscles of GRMD dogs.

Importantly, measurement of static levels of autophagic proteins in skeletal muscle does not allow definition of where the material is accumulating, nor whether there is truly increased autophagic activity or decreased autophagic flux and pathway dysregulation. So as to better make spatial distinction, we used light and transmission electron microscopy to localize LC3B positive autophagic structures in the differentially affected cranial CS and VL muscles of 6-month-old GRMD dogs. The few LC3B positive structures seen with immunofluorescence were typically in degenerating fast-twitch myofibers and invading inflammatory cells, resulting in a mixed LC3B signal indicative of muscle damage. Focal autophagic activity in degenerating myofibers could represent failed efforts (e.g., lysosome dysfunction) to save the cell or even a role in autophagic cell death (**Figure 23**). In contrast, activity in inflammatory cells may represent the necessary response to clean up dying muscle cells. Absence of LC3B and autophagosomes in non-degenerative myofibers generally matched our gene expression results, suggesting down-regulation of autophagy. These morphologic studies also highlighted the importance of utilizing a multi-modal approach to verify the cellular sources of autophagic activity in skeletal muscle.

Finally, these morphologic findings clarified our protein expression results, which indicated that autophagy is impaired in GRMD, as evidenced by higher LC3B-II and p62 levels. Autophagy likely has dual roles in dystrophic muscle, including the removal of damaged organelles and proteins, while also being involved in the inflammatory cell response to muscle injury. Furthermore, the role of autophagy varies among GRMD muscles. For example, the CS hypertrophies and stabilizes in face of impaired autophagy, while the VL atrophies. Basal autophagy dysregulation could place the fragile dystrophic myofiber at an added risk, which would be further compounded by defective cleanup of cell debris. The differential involvement of the GRMD CS emphasizes that therapeutic modulation of autophagy must be carefully considered and could require specific targeting.

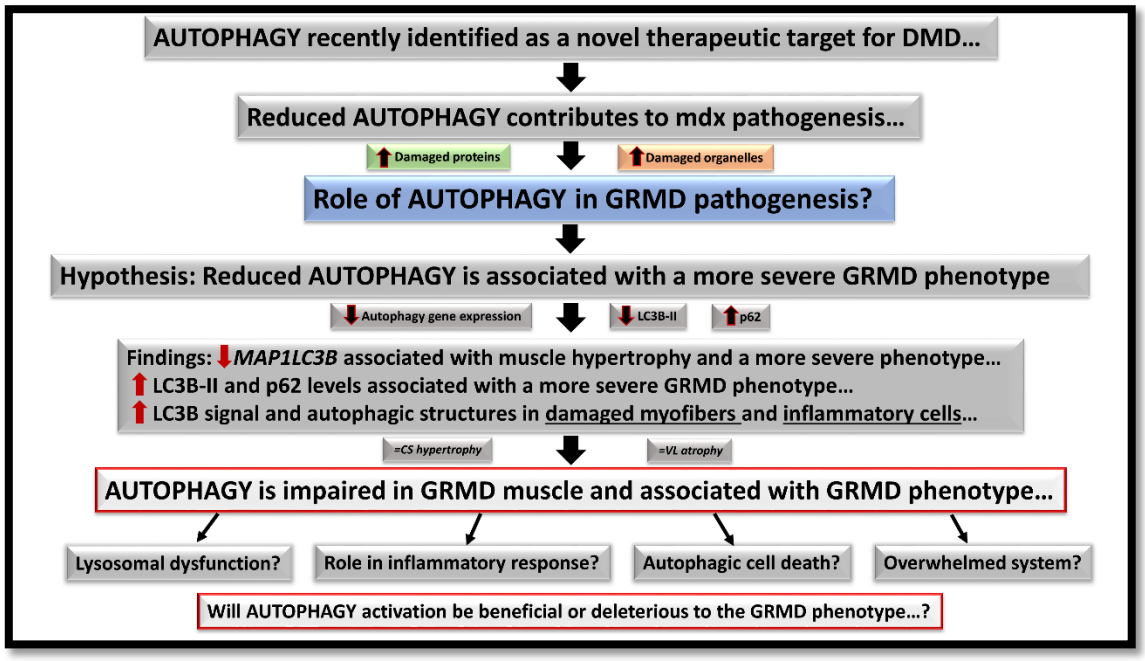

Figure 23. Schematic of the role of autophagy in GRMD pathogenesis.

Finally, we investigated the effect of NF-κB inhibition on impaired autophagy found in GRMD muscle. In light of the absence of curative therapies for DMD, treatment is often directed at ameliorating secondary effects (i.e., corticosteroids for inflammation). Drugs that inhibit NF-κB signaling have been studied extensively in a range of diseases, including DMD [96]. In particular, the Nemo binding domain (NBD) peptide blocks NF-κB by inhibiting assembly of the inhibitor of kappa B kinase (IKK) complex (i.e., IKKα and IKKβ) [97]. Mdx mice [98-100] and GRMD dogs [101] have shown improvement with NBD treatment. Interestingly, autophagy and NF-κB pathways regulate each other in a context-dependent manner, with the potential for both inhibition and induction [104-108]. However, little is known about the crosstalk between these 2 processes in dystrophic muscle.

We sought to address this void by studying autophagy gene and protein and UPS gene expression and in skeletal muscle of GRMD dogs previously treated with NBD [101]. Gene modulation in NBD treated dogs generally tracked with an improved GRMD phenotype, but this effect varied among muscles. The CS had a distinctive pattern, with gene levels being lower in GRMD versus normal dogs and increasing with NBD treatment. Higher CS gene expression implies that NBD-induced autophagy could facilitate clearance of damaged cellular debris. On the other hand, UPS gene levels tended to be lower in NBD-treated versus control GRMD dogs, consistent with reduced UPS activity and protein degradation. Such a reciprocal relationship is in keeping with the dual roles that autophagy and the UPS have in breaking down cellular components

[113] and points to the complexity of these homeostatic systems in regulating Nf-κB activity.

In summary, NBD therapy in GRMD dogs increased autophagy gene expression in a muscle-dependent manner with additional changes in autophagy protein expression. Changes in the CS, in particular, correlated with certain phenotypic makers, consistent with a beneficial effect of autophagy. In contrast, effects in the diaphragm suggested that NBD could be further exacerbating autophagy dysregulation, highlighting variable treatment effects among muscles. Therefore, treatments that modulate autophagy must be gauged to ensure that balance is restored. Further studies are required to determine the interactions between autophagy regulation and NF-κB in dystrophic skeletal muscle.

5.4 Summary

In conclusion, our investigation into the role of apoptosis and autophagy in GRMD pathogenesis has revealed several important discoveries. First, we hypothesized that protein expression of the anti-apoptotic protein APIP would be associated with an improved GRMD phenotype, supporting inhibition of apoptosis as a novel therapeutic target in DMD. However, we discovered that higher APIP expression was associated with a more severe GRMD phenotype, and furthermore, appears to be involved in the regenerative response of damaged dystrophic muscle. Second, we hypothesized that reduced autophagy would be associated with a more severe GRMD phenotype, supporting activation of autophagy as a novel therapeutic target in DMD. While our discoveries generally support this hypothesis, the variable response to impaired

autophagy in GRMD muscles (e.g., CS [hypertrophy] vs. VL [atrophy]) draws attention to the potential risks of autophagy modulation in DMD. Third, we hypothesized that treatment of GRMD dogs with NBD peptide, a novel NF-κB inhibitor, would activate autophagy and be associated with an improved GRMD phenotype. We discovered that NBD peptide therapy induced autophagy gene expression, with variable effects between individuals and muscles, some beneficial and others deleterious. Our work further highlights the importance of utilizing the GRMD dog in development and validation of novel therapeutics designed for DMD boys. It is clear that these homeostatic mechanisms are important in GRMD pathogenesis, but further studies are required to determine if apoptosis inhibition and autophagy activation will be beneficial in dystrophinopathies.

REFERENCES

[1] Emery AE. Population frequencies of inherited neuromuscular diseases--a world survey. Neuromuscul. Disord. 1991;1:19-29.

[2] Ervasti JM, Ohlendieck K, Kahl SD, Gaver MG, Campbell KP. Deficiency of a glycoprotein component of the dystrophin complex in dystrophic muscle. Nature 1990;345:315-9.

[3] Gloss D, Moxley RT, 3rd, Ashwal S, Oskoui M. Practice guideline update summary: Corticosteroid treatment of Duchenne muscular dystrophy: Report of the Guideline Development Subcommittee of the American Academy of Neurology. Neurology 2016;86:465-72.

[4] Kornegay JN, Bogan JR, Bogan DJ, et al. Canine models of Duchenne muscular dystrophy and their use in therapeutic strategies. Mamm Genome 2012;23:85-108.

[5] Sharp NJ, Kornegay JN, Van Camp SD, et al. An error in dystrophin mRNA processing in golden retriever muscular dystrophy, an animal homologue of Duchenne muscular dystrophy. Genomics 1992;13:115-21.

[6] Bushby K, Finkel R, Birnkrant DJ, et al. Diagnosis and management of Duchenne muscular dystrophy, part 1: diagnosis, and pharmacological and psychosocial management. Lancet Neurol. 2010;9:77-93.

[7] Pegoraro E, Hoffman EP, Piva L, et al. SPP1 genotype is a determinant of disease severity in Duchenne muscular dystrophy. Neurology 2011;76:219-26.

[8] Flanigan KM, Ceco E, Lamar KM, et al. LTBP4 genotype predicts age of ambulatory loss in Duchenne muscular dystrophy. Ann. Neurol. 2013;73:481-8.

[9] van den Bergen JC, Hiller M, Bohringer S, et al. Validation of genetic modifiers for Duchenne muscular dystrophy: a multicentre study assessing SPP1 and LTBP4 variants. J. Neurol. Neurosurg. Psychiatry 2015;86:1060-5.

[10] Kornegay JN, Childers MK, Bogan DJ, et al. The paradox of muscle hypertrophy in muscular dystrophy. Phys. Med. Rehabil. Clin. N. Am. 2012;23:149-72, xii.

[11] Nghiem PP, Hoffman EP, Mittal P, et al. Sparing of the dystrophin-deficient cranial sartorius muscle is associated with classical and novel hypertrophy pathways in GRMD dogs. Am. J. Pathol. 2013;183:1411-24.

[12] Vieira NM, Elvers I, Alexander MS, et al. Jagged 1 Rescues the Duchenne Muscular Dystrophy Phenotype. Cell 2015;163:1204-13.

[13] Deconinck N, Dan B. Pathophysiology of duchenne muscular dystrophy: current hypotheses. Pediatr. Neurol. 2007;36:1-7.

[14] Tidball JG, Wehling-Henricks M. Damage and inflammation in muscular dystrophy: potential implications and relationships with autoimmune myositis. Curr. Opin. Rheumatol. 2005;17:707-13.

[15] Sprick MR, Walczak H. The interplay between the Bcl-2 family and death receptor-mediated apoptosis. Biochim. Biophys. Acta 2004;1644:125-32.

[16] Tews DS. Muscle-fiber apoptosis in neuromuscular diseases. Muscle Nerve 2005;32:443-58.

[17] Sandri M, Carraro U. Apoptosis of skeletal muscles during development and disease. Int. J. Biochem. Cell Biol. 1999;31:1373-90.

[18] Dominov JA, Houlihan-Kawamoto CA, Swap CJ, Miller JB. Pro- and anti-apoptotic members of the Bcl-2 family in skeletal muscle: a distinct role for Bcl-2 in later stages of myogenesis. Dev. Dyn. 2001;220:18-26.

[19] Reutenauer J, Dorchies OM, Patthey-Vuadens O, Vuagniaux G, Ruegg UT. Investigation of Debio 025, a cyclophilin inhibitor, in the dystrophic mdx mouse, a model for Duchenne muscular dystrophy. Br. J. Pharmacol. 2008;155:574-84.

[20] Wissing ER, Millay DP, Vuagniaux G, Molkentin JD. Debio-025 is more effective than prednisone in reducing muscular pathology in mdx mice. Neuromuscul. Disord. 2010;20:753-60.

[21] Mizushima N, Levine B, Cuervo AM, Klionsky DJ. Autophagy fights disease through cellular self-digestion. Nature 2008;451:1069-75.

[22] Romanello V, Sandri M. Mitochondrial Quality Control and Muscle Mass Maintenance. Front. Physiol. 2015;6:422.

[23] Choi AM, Ryter SW, Levine B. Autophagy in human health and disease. N. Engl. J. Med. 2013;368:651-62.

[24] Klionsky DJ, Abdelmohsen K, Abe A, et al. Guidelines for the use and interpretation of assays for monitoring autophagy (3rd edition). Autophagy 2016;12:1-222.

[25] Terman A, Brunk UT. Oxidative stress, accumulation of biological 'garbage', and aging. Antioxid Redox Signal 2006;8:197-204.

[26] Partridge TA. Cells that participate in regeneration of skeletal muscle. Gene Ther 2002;9:752-3.

[27] Sandri M, Coletto L, Grumati P, Bonaldo P. Misregulation of autophagy and protein degradation systems in myopathies and muscular dystrophies. J. Cell Sci. 2013;126:5325-33.

[28] Masiero E, Agatea L, Mammucari C, et al. Autophagy is required to maintain muscle mass. Cell Metab 2009;10:507-15.

[29] Koo T, Wood MJ. Clinical trials using antisense oligonucleotides in duchenne muscular dystrophy. Hum. Gene Ther. 2013;24:479-88.

[30] Jacobson RD, Feldman EL. Antisense Oligonucleotides for Duchenne Muscular Dystrophy: Why No Neurologist Should Skip This. JAMA Neurol. 2016;73:259-60.

[31] Porter JD, Khanna S, Kaminski HJ, et al. A chronic inflammatory response dominates the skeletal muscle molecular signature in dystrophin-deficient mdx mice. Hum. Mol. Genet. 2002;11:263-72.

[32] Baron D, Magot A, Ramstein G, et al. Immune response and mitochondrial metabolism are commonly deregulated in DMD and aging skeletal muscle. PloS One 2011;6:e26952.

[33] Turk R, Sterrenburg E, de Meijer EJ, van Ommen GJ, den Dunnen JT, t Hoen PA. Muscle regeneration in dystrophin-deficient mdx mice studied by gene expression profiling. BMC Genomics 2005;6:98.

[34] Brinkmeyer-Langford C, Balog-Alvarez C, Cai JJ, Davis BW, Kornegay JN. Genome-wide association study to identify potential genetic modifiers in a canine model for Duchenne muscular dystrophy. BMC Genomics 2016;17:665.

[35] Cho DH, Hong YM, Lee HJ, et al. Induced inhibition of ischemic/hypoxic injury by APIP, a novel Apaf-1-interacting protein. J. Biol. Chem. 2004;279:39942-50.

[36] Cho DH, Lee HJ, Kim HJ, et al. Suppression of hypoxic cell death by APIP-induced sustained activation of AKT and ERK1/2. Oncogene 2007;26:2809-14.

[37] Rando TA. Oxidative stress and the pathogenesis of muscular dystrophies. Am. J. Phys. Med. Rehabil. 2002;81:S175-86.

[38] Tews DS. Characterization of initiator and effector caspase expressions in dystrophinopathies. Neuropathology 2006;26:24-31.

[39] Olive M, Ferrer I. Bcl-2 and Bax protein expression in human myopathies. J. Neurol. Sci. 1999;164:76-81.

[40] Dominov JA, Kravetz AJ, Ardelt M, Kostek CA, Beermann ML, Miller JB. Muscle-specific BCL2 expression ameliorates muscle disease in laminin {alpha}2-deficient, but not in dystrophin-deficient, mice. Hum. Mol. Genet. 2005;14:1029-40.

[41] Kornegay JN, Bogan JR, Bogan DJ, Childers MK, Grange RW. Golden retriever muscular dystrophy (GRMD): Developing and maintaining a colony and physiological functional measurements. Methods Mol. Biol. 2011;709:105-23.

[42] Kornegay JN, Bogan DJ, Bogan JR, et al. Contraction force generated by tarsal joint flexion and extension in dogs with golden retriever muscular dystrophy. J. Neurol. Sci. 1999;166:115-21.

[43] Kornegay JN, Cundiff DD, Bogan DJ, Bogan JR, Okamura CS. The cranial sartorius muscle undergoes true hypertrophy in dogs with golden retriever muscular dystrophy. Neuromuscul. Disord. 2003;13:493-500.

[44] Bartlett RJ, Winand NJ, Secore SL, et al. Mutation segregation and rapid carrier detection of X-linked muscular dystrophy in dogs. Am. J. Vet. Res. 1996;57:650-4.

[45] Markwell MA, Haas SM, Bieber LL, Tolbert NE. A modification of the Lowry procedure to simplify protein determination in membrane and lipoprotein samples. Anal. Biochem. 1978;87:206-10.

[46] Tidball JG, Albrecht DE, Lokensgard BE, Spencer MJ. Apoptosis precedes necrosis of dystrophin-deficient muscle. J. Cell Sci. 1995;108 (Pt 6):2197-204.

[47] Barnes BT, Confides AL, Rich MM, Dupont-Versteegden EE. Distinct muscle apoptotic pathways are activated in muscles with different fiber types in a rat model of critical illness myopathy. J. Muscle Res. Cell Motil. 2015;36:243-53.

[48] McMillan EM, Quadrilatero J. Differential apoptosis-related protein expression, mitochondrial properties, proteolytic enzyme activity, and DNA fragmentation between skeletal muscles. Am. J. Physiol. Regul. Integr. Comp. Physiol. 2011;300:R531-43.

[49] Armstrong RB, Saubert CWt, Seeherman HJ, Taylor CR. Distribution of fiber types in locomotory muscles of dogs. Am. J. Anat. 1982;163:87-98.

[50] Ko DC, Gamazon ER, Shukla KP, et al. Functional genetic screen of human diversity reveals that a methionine salvage enzyme regulates inflammatory cell death. Proc. Natl. Acad. Sci. U. S. A. 2012;109:E2343-52.

[51] Mary C, Duek P, Salleron L, et al. Functional identification of APIP as human mtnB, a key enzyme in the methionine salvage pathway. PloS One 2012;7:e52877.

[52] Kang W, Hong SH, Lee HM, et al. Structural and biochemical basis for the inhibition of cell death by APIP, a methionine salvage enzyme. Proc. Natl. Acad. Sci. U. S. A. 2014;111:E54-61.

[53] Tang B, Kadariya Y, Murphy ME, Kruger WD. The methionine salvage pathway compound 4-methylthio-2-oxobutanate causes apoptosis independent of down-regulation of ornithine decarboxylase. Biochem. Pharmacol. 2006;72:806-15.

[54] Li TW, Zhang Q, Oh P, et al. S-Adenosylmethionine and methylthioadenosine inhibit cellular FLICE inhibitory protein expression and induce apoptosis in colon cancer cells. Mol. Pharmacol. 2009;76:192-200.

[55] Kadariya Y, Yin B, Tang B, et al. Mice heterozygous for germ-line mutations in methylthioadenosine phosphorylase (MTAP) die prematurely of T-cell lymphoma. Cancer Res. 2009;69:5961-9.

[56] Wright FA, Strug LJ, Doshi VK, et al. Genome-wide association and linkage identify modifier loci of lung disease severity in cystic fibrosis at 11p13 and 20q13.2. Nat. Genet. 2011;43:539-46.

[57] Jarvinen AK, Autio R, Kilpinen S, et al. High-resolution copy number and gene expression microarray analyses of head and neck squamous cell carcinoma cell lines of tongue and larynx. Genes Chromosomes Cancer 2008;47:500-9.

[58] De Palma C, Morisi F, Cheli S, et al. Autophagy as a new therapeutic target in Duchenne muscular dystrophy. Cell Death Dis. 2012;3:e418.

[59] Bibee KP, Cheng YJ, Ching JK, et al. Rapamycin nanoparticles target defective autophagy in muscular dystrophy to enhance both strength and cardiac function. FASEB J 2014;28:2047-61.

[60] Pauly M, Daussin F, Burelle Y, et al. AMPK activation stimulates autophagy and ameliorates muscular dystrophy in the mdx mouse diaphragm. Am. J. Pathol. 2012;181:583-92.

[61] Spitali P, Grumati P, Hiller M, Chrisam M, Aartsma-Rus A, Bonaldo P. Autophagy is Impaired in the Tibialis Anterior of Dystrophin Null Mice. PLoS Curr 2013;5.

[62] Pal R, Palmieri M, Loehr JA, et al. Src-dependent impairment of autophagy by oxidative stress in a mouse model of Duchenne muscular dystrophy. Nat Commun 2014;5:4425.

[63] Hindi SM, Sato S, Choi Y, Kumar A. Distinct roles of TRAF6 at early and late stages of muscle pathology in the mdx model of Duchenne muscular dystrophy. Hum Mol Genet 2014;23:1492-505.

[64] Young CN, Sinadinos A, Lefebvre A, et al. A novel mechanism of autophagic cell death in dystrophic muscle regulated by P2RX7 receptor large-pore formation and HSP90. Autophagy 2015;11:113-30.

[65] Peter AK, Crosbie RH. Hypertrophic response of Duchenne and limb-girdle muscular dystrophies is associated with activation of Akt pathway. Exp Cell Res 2006;312:2580-91.

[66] Dogra C, Changotra H, Wergedal JE, Kumar A. Regulation of phosphatidylinositol 3-kinase (PI3K)/Akt and nuclear factor-kappa B signaling pathways in dystrophin-deficient skeletal muscle in response to mechanical stretch. J. Cell. Physiol. 2006;208:575-85.

[67] Mammucari C, Milan G, Romanello V, et al. FoxO3 controls autophagy in skeletal muscle in vivo. Cell Metab 2007;6:458-71.

[68] Patronek GJ, Waters DJ, Glickman LT. Comparative longevity of pet dogs and humans: implications for gerontology research. J. Gerontol. A Biol. Sci. Med. Sci. 1997;52:B171-8.

[69] Ruijter JM, Lorenz P, Tuomi JM, Hecker M, van den Hoff MJ. Fluorescent-increase kinetics of different fluorescent reporters used for qPCR depend on monitoring chemistry, targeted sequence, type of DNA input and PCR efficiency. Mikrochim. Acta 2014;181:1689-1696.

[70] Ruijter JM, Ramakers C, Hoogaars WM, et al. Amplification efficiency: linking baseline and bias in the analysis of quantitative PCR data. Nucleic Acids Res. 2009;37:e45.

[71] Tuomi JM, Voorbraak F, Jones DL, Ruijter JM. Bias in the Cq value observed with hydrolysis probe based quantitative PCR can be corrected with the estimated PCR efficiency value. Methods 2010;50:313-22.

[72] Schmittgen TD, Livak KJ. Analyzing real-time PCR data by the comparative C(T) method. Nat. Protoc. 2008;3:1101-8.

[73] Mofarrahi M, Guo Y, Haspel JA, et al. Autophagic flux and oxidative capacity of skeletal muscles during acute starvation. Autophagy 2013;9:1604-20.

[74] Weidberg H, Shvets E, Shpilka T, Shimron F, Shinder V, Elazar Z. LC3 and GATE-16/GABARAP subfamilies are both essential yet act differently in autophagosome biogenesis. EMBO J. 2010;29:1792-802.

[75] Mizushima N, Noda T, Yoshimori T, et al. A protein conjugation system essential for autophagy. Nature 1998;395:395-8.

[76] Kang R, Zeh HJ, Lotze MT, Tang D. The Beclin 1 network regulates autophagy and apoptosis. Cell Death Differ. 2011;18:571-80.

[77] Hanna RA, Quinsay MN, Orogo AM, Giang K, Rikka S, Gustafsson AB. Microtubule-associated protein 1 light chain 3 (LC3) interacts with Bnip3 protein to selectively remove endoplasmic reticulum and mitochondria via autophagy. J. Biol. Chem. 2012;287:19094-104.

[78] Bodine SC, Latres E, Baumhueter S, et al. Identification of ubiquitin ligases required for skeletal muscle atrophy. Science 2001;294:1704-8.

[79] Wang Y, Pessin JE. Mechanisms for fiber-type specificity of skeletal muscle atrophy. Curr. Opin. Clin. Nutr. Metab. Care 2013;16:243-50.

[80] Webster C, Silberstein L, Hays AP, Blau HM. Fast muscle fibers are preferentially affected in Duchenne muscular dystrophy. Cell 1988;52:503-13.

[81] Selsby JT, Morine KJ, Pendrak K, Barton ER, Sweeney HL. Rescue of dystrophic skeletal muscle by PGC-1alpha involves a fast to slow fiber type shift in the mdx mouse. PloS One 2012;7:e30063.

[82] Yang DS, Lee JH, Nixon RA. Monitoring autophagy in Alzheimer's disease and related neurodegenerative diseases. Methods Enzymol. 2009;453:111-44.

[83] Edinger AL, Thompson CB. Death by design: apoptosis, necrosis and autophagy. Curr. Opin. Cell Biol. 2004;16:663-9.

[84] Bodine SC, Stitt TN, Gonzalez M, et al. Akt/mTOR pathway is a crucial regulator of skeletal muscle hypertrophy and can prevent muscle atrophy in vivo. Nat. Cell Biol. 2001;3:1014-9.

[85] Gurpur PB, Liu J, Burkin DJ, Kaufman SJ. Valproic acid activates the PI3K/Akt/mTOR pathway in muscle and ameliorates pathology in a mouse model of Duchenne muscular dystrophy. Am. J. Pathol. 2009;174:999-1008.

[86] Duguez S, Duddy W, Johnston H, et al. Dystrophin deficiency leads to disturbance of LAMP1-vesicle-associated protein secretion. Cell. Mol. Life Sci. 2013;70:2159-74.

[87] Levine B, Kroemer G. Autophagy in the pathogenesis of disease. Cell 2008;132:27-42.

[88] Martinez J, Almendinger J, Oberst A, et al. Microtubule-associated protein 1 light chain 3 alpha (LC3)-associated phagocytosis is required for the efficient clearance of dead cells. Proc. Natl. Acad. Sci. U. S. A. 2011;108:17396-401.

[89] Martinez J, Malireddi RK, Lu Q, et al. Molecular characterization of LC3-associated phagocytosis reveals distinct roles for Rubicon, NOX2 and autophagy proteins. Nat. Cell Biol. 2015;17:893-906.

[90] Sanjuan MA, Dillon CP, Tait SW, et al. Toll-like receptor signalling in macrophages links the autophagy pathway to phagocytosis. Nature 2007;450:1253-7.

[91] Monaco AP, Neve RL, Colletti-Feener C, Bertelson CJ, Kurnit DM, Kunkel LM. Isolation of candidate cDNAs for portions of the Duchenne muscular dystrophy gene. Nature 1986;323:646-50.

[92] Burghes AH, Logan C, Hu X, Belfall B, Worton RG, Ray PN. A cDNA clone from the Duchenne/Becker muscular dystrophy gene. Nature 1987;328:434-7.

[93] Hoffman EP, Brown RH, Jr., Kunkel LM. Dystrophin: the protein product of the Duchenne muscular dystrophy locus. Cell 1987;51:919-28.

[94] Kornegay JN, Spurney CF, Nghiem PP, Brinkmeyer-Langford CL, Hoffman EP, Nagaraju K. Pharmacologic management of Duchenne muscular dystrophy: target identification and preclinical trials. ILAR J 2014;55:119-49.

[95] Monici MC, Aguennouz M, Mazzeo A, Messina C, Vita G. Activation of nuclear factor-kappaB in inflammatory myopathies and Duchenne muscular dystrophy. Neurology 2003;60:993-7.

[96] Gilmore TD, Herscovitch M. Inhibitors of NF-kappaB signaling: 785 and counting. Oncogene 2006;25:6887-99.

[97] Strickland I, Ghosh S. Use of cell permeable NBD peptides for suppression of inflammation. Ann. Rheum. Dis. 2006;65 Suppl 3:iii75-82.

[98] Acharyya S, Villalta SA, Bakkar N, et al. Interplay of IKK/NF-kappaB signaling in macrophages and myofibers promotes muscle degeneration in Duchenne muscular dystrophy. J. Clin. Invest. 2007;117:889-901.

[99] Peterson JM, Kline W, Canan BD, et al. Peptide-based inhibition of NF-kappaB rescues diaphragm muscle contractile dysfunction in a murine model of Duchenne muscular dystrophy. Mol. Med. 2011;17:508-15.

[100] Reay DP, Yang M, Watchko JF, et al. Systemic delivery of NEMO binding domain/IKKgamma inhibitory peptide to young mdx mice improves dystrophic skeletal muscle histopathology. Neurobiol. Dis. 2011;43:598-608.

[101] Kornegay JN, Peterson JM, Bogan DJ, et al. NBD delivery improves the disease phenotype of the golden retriever model of Duchenne muscular dystrophy. Skelet Muscle 2014;4:18.

[102] De Palma C, Perrotta C, Pellegrino P, Clementi E, Cervia D. Skeletal muscle homeostasis in duchenne muscular dystrophy: modulating autophagy as a promising therapeutic strategy. Front. Aging Neurosci. 2014;6:188.

[103] Whitehead NP, Kim MJ, Bible KL, Adams ME, Froehner SC. A new therapeutic effect of simvastatin revealed by functional improvement in muscular dystrophy. Proc. Natl. Acad. Sci. U. S. A. 2015;112:12864-9.

[104] Salminen A, Hyttinen JM, Kauppinen A, Kaarniranta K. Context-Dependent Regulation of Autophagy by IKK-NF-kappaB Signaling: Impact on the Aging Process. Int. J. Cell Biol. 2012;2012:849541.

[105] Nivon M, Richet E, Codogno P, Arrigo AP, Kretz-Remy C. Autophagy activation by NFkappaB is essential for cell survival after heat shock. Autophagy 2009;5:766-83.

[106] Djavaheri-Mergny M, Amelotti M, Mathieu J, et al. NF-kappaB activation represses tumor necrosis factor-alpha-induced autophagy. J. Biol. Chem. 2006;281:30373-82.

[107] Djavaheri-Mergny M, Amelotti M, Mathieu J, Besancon F, Bauvy C, Codogno P. Regulation of autophagy by NFkappaB transcription factor and reactives oxygen species. Autophagy 2007;3:390-2.

[108] Trocoli A, Djavaheri-Mergny M. The complex interplay between autophagy and NF-kappaB signaling pathways in cancer cells. Am. J. Cancer Res. 2011;1:629-49.

[109] Wadosky KM, Li L, Rodriguez JE, et al. Regulation of the calpain and ubiquitin-proteasome systems in a canine model of muscular dystrophy. Muscle Nerve 2011;44:553-62.

[110] Pandey UB, Nie Z, Batlevi Y, et al. HDAC6 rescues neurodegeneration and provides an essential link between autophagy and the UPS. Nature 2007;447:859-63.

[111] Nedelsky NB, Todd PK, Taylor JP. Autophagy and the ubiquitin-proteasome system: collaborators in neuroprotection. Biochim. Biophys. Acta 2008;1782:691-9.

[112] Iwata A, Riley BE, Johnston JA, Kopito RR. HDAC6 and microtubules are required for autophagic degradation of aggregated huntingtin. J. Biol. Chem. 2005;280:40282-92.

[113] Zhao J, Brault JJ, Schild A, Goldberg AL. Coordinate activation of autophagy and the proteasome pathway by FoxO transcription factor. Autophagy 2008;4:378-80.

[114] Vogel C, Marcotte EM. Insights into the regulation of protein abundance from proteomic and transcriptomic analyses. Nat Rev Genet 2012;13:227-32.

[115] Zhong Z, Umemura A, Sanchez-Lopez E, et al. NF-kappaB Restricts Inflammasome Activation via Elimination of Damaged Mitochondria. Cell 2016;164:896-910.

[116] Barnes PJ, Karin M. Nuclear factor-kappaB: a pivotal transcription factor in chronic inflammatory diseases. N. Engl. J. Med. 1997;336:1066-71.

[117] Greten FR, Arkan MC, Bollrath J, et al. NF-kappaB is a negative regulator of IL-1beta secretion as revealed by genetic and pharmacological inhibition of IKKbeta. Cell 2007;130:918-31.